1989

Harmonic Measurement and Reduction in Power Systems.

Rutisurhata Kurniawan Hartana
Louisiana State University and Agricultural & Mechanical College

Order Number 9025310

Harmonic measurement and reduction in power systems

Hartana, Rutisurhata Kurniawan, Ph.D.

The Louisiana State University and Agricultural and Mechanical Col., 1989

U·M·I

300 N. Zeeb Rd.
Ann Arbor, MI 48106

HARMONIC MEASUREMENT AND REDUCTION IN POWER SYSTEMS

A Dissertation

Submitted to the Graduate Faculty of the
Louisiana State University and
Agricultural and Mechanical College
in partial fulfillment of the
requirements for the degree of
Doctor of Philosophy

in

The Department of Electrical and Computer Engineering

by
Rutisurhata K. Hartana
Engineer, Trisakti University, 1982
M.S., Louisiana State University, 1983
December 1989

ACKNOWLEDGMENTS

The author wishes to express his gratitude and appreciation to Dr. Gill G. Richards for his unique friendship and guidance throughout the author's graduate program and his valuable assistance in the preparation of this dissertation. Appreciation is also expressed to Dr. Owen T. Tan for his assistance and guidance, Dr. Subhash C. Kak and Dr. Jerry L. Trahan of the Electrical and Computer Engineering Department, and Dr. James R. Dorroh of the Mathematics Department for serving as members of the examining committee.

The financial assistance of the Electrical and Computer Engineering Department and the Electric Power Research Consortium, sponsored by Louisiana Power and Light Co., Gulf States Utilities Co., and Central Louisiana Electric Co., is greatly acknowledged.

The author would like to express his deepest appreciation to his parents, his sisters and brothers for their love and support throughout his studies. Finally, the author wishes to thank his friend, N. Iwan Santoso (who is also a candidate for the degree of Doctor of Philosophy in Electrical Engineering), for his constant friendship and encouragement, and to gratefully acknowledge the assistance of Dr. Ali Mirbod and Dr. Powsiri Klinkhachorn during his graduate studies.

TABLE OF CONTENTS

LIST OF TABLES

LIST OF FIGURES

ABSTRACT

Harmonic voltages and currents are created by nonlinear loads in power systems. These harmonics can cause serious problems to the energy suppliers (utility companies) and energy users (consumers). This dissertation presents new techniques for harmonic measurement and the accompanying problem, harmonic reduction.

To reduce harmonics, the location and magnitude of harmonic sources must be known a priori. However, to measure and monitor harmonic sources requires specialized instrumentation that is not generally permanently installed at most buses. In this study, a method is developed to use neural networks in conjunction with state estimation for monitoring and estimating harmonic sources with only a few permanent instruments. The method can also identify and monitor a "suspected" harmonic source that has not previously been measured.

Once harmonic sources are known, the objective from an energy supplier's point of view is to minimize the combined total harmonic distortion of all buses on a distribution system. A procedure is developed for designing optimum filters on distribution feeders that have distributed and balanced or unbalanced harmonic sources and variable compensating capacitors. The design includes finding optimum filter admittances and the corresponding locations. Symmetrical components are used for the unbalanced harmonic source case. Filter realization with the lowest cost including sensitivity analysis is also discussed. The optimum filters chosen and placed in this manner may produce results superior to the conventional filter design procedures.

The problem of harmonic reduction is alternatively approached as an energy user's problem. The user's objective is to eliminate his voltage harmonic distortion problem locally without considering the effects of voltage distortion at neighboring buses. The remedy is insertion of a reactor in series with the local compensating capacitor. A method is presented for finding the optimum fixed *LC* combination to minimize voltage harmonic

distortion at a load bus while holding the displacement factor (fundamental power factor) at a desired value and constraining the total cost of the compensating equipment. Source harmonics and impedances are represented as randomly time-varying quantities.

CHAPTER 1
INTRODUCTION

The problem of power system harmonics has been recognized at least since the early 1930's when distorted voltage and current waveforms were observed on transmission lines and electric equipment [1]. At that time, the sources of harmonics were limited to synchronous and induction machines and saturated transformers. However, in more recent years, the number of nonlinear loads used by power utilities and consumers has grown rapidly because of the advances in high power semiconductor switching devices. AC/DC and DC/AC power converters which are widely used in high voltage direct current (HVDC) transmission, motor speed control, uninterrupted power supplies (UPS), traction-power stations, battery chargers, and photovoltaic stations, as well as arc furnaces, arc welders, arc lighting, fluorescent lamps, TV receivers, and static VAR compensators, have reawakened interest in power system harmonics [1-5].

Harmonic voltages and currents can cause many serious operational problems to both energy suppliers and users. Some of the major effects of harmonics include: overvoltages and excessive currents due to resonances between system impedances and compensating capacitors, power factor degradation, insulation degradation, capacitor bank failure, mechanical oscillation and excessive heating of electric machines, interference with ripple control systems, metering errors such as in induction watthour meter, interference with communication systems, relay malfunction, and unstable operation of firing circuits based on zero voltage crossing detection [3-13]. Therefore, there is growing interest in the power industry today in reducing the increasing levels of harmonic distortion.

Harmonic distortion in a power system is investigated by harmonic measurement and computer simulation. Several digital computer simulations for analyzing the propagation of harmonic currents into the power network are in use. The procedure may be a Newton-Raphson based harmonic power flow technique [14-16] or a technique based on

the current injection response of the network [17-21]. In these methods, the location and magnitude of harmonic sources must be known a priori. However, if they are not known, a practical engineering question may be to identify the location and type of the harmonic sources by measurement. Therefore, harmonic measurement is an integral part of harmonic analysis and reduction. The methodology and instrumentation of harmonic measurements are discussed in Refs [3,4,22,23]. Harmonic measurements provide background information on system harmonic levels which can be used to verify the simulation model being used. However, harmonic measurements on high voltage systems require specialized instrumentation such as voltage/current transducers and harmonic/spectrum analyzers [24,25] that are relatively expensive.

A complete measurement of harmonics in a power system was obtained in Ref. [26] by state estimation, but a relatively large number of harmonic detectors had to be placed throughout the system if the harmonic sources are to be monitored continuously. Because of its high cost, inconvenience and complexity, harmonic instrumentation in a typical system may only supply a few measurements of harmonic flows or injections, which may be insufficient to monitor all harmonic sources. Therefore, it is necessary to be able to estimate harmonic sources using relatively few permanently instrumented buses. This subject is the first issue to be addressed in this study.

Harmonic currents injected into a power distribution system may cause unexpected voltage harmonic distortion (overvoltage) among users, even the ones which do not produce harmonics. Such distortion is mainly caused by resonances between system impedances and compensating capacitors [4,8]. Therefore, the energy supplier may wish to reduce it. The usual approach to reducing voltage harmonic distortion by the energy supplier is to select a filter and place it at the most distorted bus. The commonly used harmonic filter is the resonant shunt (tuned) filter. The design of such a filter including its rating and cost is discussed in Refs [4,6,27]. This type of filtering is applicable when there is only one major harmonic source to be filtered, but it may actually cause worse distortion

at other buses on the same distribution feeder, especially when there are several harmonic sources.

Since filtering the largest harmonic source may not be optimal for all utility customers, it may be desirable for an energy supplier to minimize voltage distortion for an entire feeder. Techniques for such feeder filtering are discussed in Refs [28-30], but the solution approach is qualitative and intuitive, rather than quantitative. The subject of distortion caused by distributed harmonic sources on feeders is also discussed in Ref. [31], which suggests that distortion can be associated with an entire distribution feeder, rather than a single bus.

If the entire feeder is to be filtered, the problems of shifting system response caused by variable (switchable) compensating capacitors and filter placement must be taken into account. It is suggested in Refs [28-30] that the filters be selected with switched capacitor banks at their "worst case" values. The search for the worst case is an exhaustive search of all possible resonant conditions. After placing the filter, the search is done again to assure that there is no new resonance. This approach requires iteration and may not converge. The problem of filter placement is also discussed in Refs [28-30], which suggest the simple rule of placing the filter at the capacitor bank farthest from the substation. However, this rule is not always best for the case of distributed harmonic sources. These problems and their solution are the second topic in this study.

The harmonic problem can be alternatively approached as an energy user's problem. The user's objective is to eliminate his own voltage harmonic distortion without including the effects of voltage distortion at neighboring buses. It is assumed that the harmonic currents injected by the user's nonlinear load are not sufficiently serious to suggest tuned filters. Therefore, when harmonic distortion is clearly caused by the local compensating capacitor, a first reaction might be to change the capacitor value while still retaining sufficient fundamental compensation [32]. Refs [33-35] showed that source-generated harmonics could be reduced by inserting an optimal reactor in series with the

compensating capacitor, while a higher maximum possible power factor is also obtained. Furthermore, if a sufficiently complex compensation network is used, current harmonics can be completely eliminated as shown in Refs [36-38]. In these papers, the main objective is to correct (compensate) the load power factor under nonsinusoidal conditions. However, correcting the power factor does not necessarily minimize voltage harmonic distortion.

In addition, a constant load can not be assumed in selecting an optimum compensator. Harmonics generated in distribution systems, particularly at the residential and commercial levels, are generally time-varying at random due to stochastic changes in the operating modes of nonlinear loads [1,39,40]. The system impedances are also constantly changing because of capacitor switching and load changes within the distribution system. It is shown in Refs [35,41-43] that the design of an optimum C or LC compensator must take into account statistical properties of harmonic system parameters and sources. The problem of reducing voltage harmonic distortion at a local load bus while maintaining a given displacement factor (fundamental power factor) and taking into account time variations of harmonics and impedances is the third topic of this study.

This dissertation is arranged into four chapters: Chapter 2 presents a survey of harmonic analysis including modeling of harmonic sources and other components in power systems. The existing analytical methods and computer programs for analyzing harmonic propagation and flow into the power network are discussed. Harmonic measurement and several techniques for harmonic reduction and control are also explained.

Chapter 3 discusses the harmonic measurement problem: to monitor and identify harmonic sources with relatively few permanent harmonic measuring instruments [44]. Neural networks are applied to make initial estimates of harmonic sources in a power system with nonlinear loads. The neural network estimates are then used as pseudomeasurements for harmonic state estimation, which further improves the measurements. The method is also applied to monitor and identify an unknown harmonic source.

Chapter 4 discusses the harmonic reduction problem that is faced by an energy supplier: to design optimum filters on distribution feeders that have distributed and balanced or unbalanced harmonic sources and variable compensating capacitors [45]. The objective is to minimize the whole feeder voltage harmonic distortion. First, a measure of combined total harmonic distortion for the entire feeder buses is introduced and a method of finding optimum filter admittances with varying compensating capacitors is developed. Symmetrical components are used for the unbalanced harmonic source case. Then, the problem of filter placement is explored. Finally, filter realization with the lowest cost (size) including sensitivity analysis, is discussed. An example distribution feeder is simulated and the results are compared to the conventional filter design procedures.

Chapter 5 discusses the harmonic reduction problem from the user's point of view. A method is presented for finding an optimum fixed *LC* compensator to minimize voltage harmonic distortion at a local load bus while holding the displacement factor at a desired value [46]. The total size and corresponding cost of the compensating equipment is constrained and minimized. Source harmonics and impedances are represented as randomly time-varying quantities. In this study, a cost function for the harmonic reduction approach is first introduced as the objective function to be minimized. The expression, analysis and optimization of the objective function are then discussed. Finally, the results of a network simulation test with *LC* compensator are compared with the performance and cost of purely capacitive compensation.

CHAPTER 2

OVERVIEW OF HARMONICS IN POWER SYSTEMS

This chapter presents a brief review of power system harmonics including modeling of harmonic sources and other power system components, analytical and computer methods for harmonic analysis, harmonic measurement and instrumentation, and techniques for harmonic reduction and control.

2.1 Harmonic Modeling

The discussion of harmonic modeling is arranged into two parts. The first part deals with the sources of harmonics or harmonic-producing (nonlinear) loads. The second part describes the equivalent circuit models of various power system components.

2.1.1 Harmonic Sources

The increase of harmonic signals in power systems is primarily attributed to the increased use of power system components whose nonlinear operating characteristics result in the generation of harmonics. The most commonly known power apparatus that generate harmonics are power semiconductor devices, particularly static power converters, since they are widely used for power system conditioning applications with a wide range of power ratings.

2.1.1.1 Static Power Converters

Static power converters can be classified into three different groups according to their power ratings: large power converters (rated in MW), medium size converters (rated in tens and hundreds of kW) and low power converters.

Large Power Converters

Large power converters are used in the metal industry and high voltage direct

current (HVDC) transmission. They generally have large inductance on the dc side. The direct current is thus reasonably constant and the converter acts like a harmonic current source on the ac side. Depending on the value of thyristor firing angle, the converter can be utilized as a rectifier (ac to dc conversion) or as an inverter (dc to ac conversion). The equivalent circuits of a rectifier and an inverter are shown in Fig. 2.1(a) and 2.1(b), respectively [3,17].

A converter of pulse number p generates characteristic current harmonics of orders

$$h = pn \pm 1, \qquad n = 1, 2, 3, \ldots\ldots \tag{2.1}$$

on the ac side, with their rms values given by [4,6]

$$I_h = \frac{I_1}{h} = \frac{1}{h}\frac{\sqrt{6}\, I_d}{\pi} \tag{2.2}$$

where I_1 is the rms value of the fundamental current and I_d is the converter direct current. Z_h (as shown in Fig. 2.1) is the equivalent h-th harmonic impedance. It is assumed here that the commutation occurs instantly, that is, without overlap.

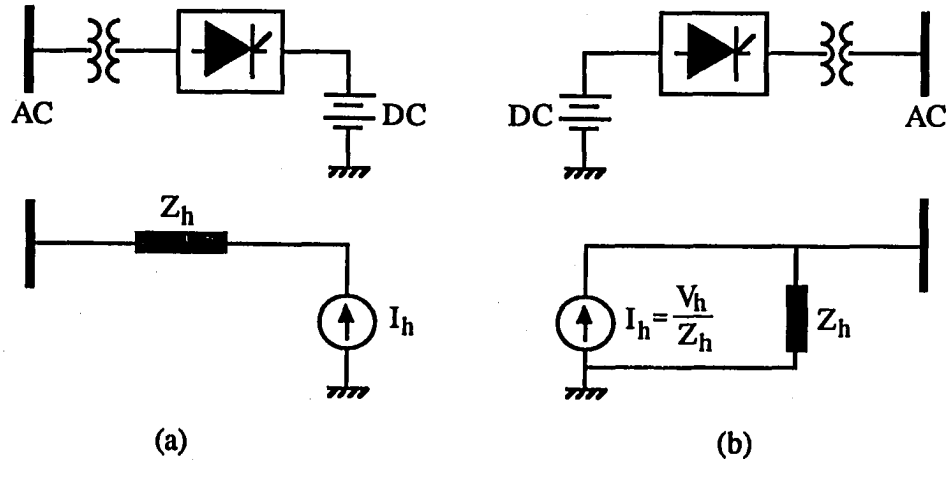

Fig. 2.1 Equivalent Circuit of Converter: (a) Rectifier, and (b) Inverter

For a 6-pulse converter with a Y-Y connected transformer, the frequency domain representation of line current in phase 'a' is

$$i_a(t) = \frac{2\sqrt{3}}{\pi} I_d \left\{ \cos(\omega t) - \tfrac{1}{5}\cos(5\omega t) + \tfrac{1}{7}\cos(7\omega t) - \tfrac{1}{11}\cos(11\omega t) + \tfrac{1}{13}\cos(13\omega t) - \ldots\ldots\ldots \right\}. \quad (2.3)$$

If either the primary or secondary 3-phase windings of the converter transformer are connected in delta, the line current in phase 'a' of eqn (2.3) becomes

$$i_a(t) = \frac{2\sqrt{3}}{\pi} I_d \left\{ \cos(\omega t) + \tfrac{1}{5}\cos(5\omega t) - \tfrac{1}{7}\cos(7\omega t) - \tfrac{1}{11}\cos(11\omega t) + \tfrac{1}{13}\cos(13\omega t) + \ldots\ldots\ldots \right\}. \quad (2.4)$$

When the commutation (overlap) angle is not neglected, the magnitude of the h-th harmonic current is [6]

$$I_h = \frac{I_1}{h\,D} F(\alpha, \mu) \quad (2.5)$$

where

$$D = \cos\alpha - \cos(\alpha + \mu),$$

$$F(\alpha, \mu) = \left[A_1^2 + A_2^2 - 2 A_1 A_2 \cos(2\alpha + \mu) \right]^{\frac{1}{2}},$$

$$A_1 = \frac{\sin\left\{(h-1)\frac{\mu}{2}\right\}}{h-1},$$

$$A_2 = \frac{\sin\left\{(h+1)\frac{\mu}{2}\right\}}{h+1}, \quad (2.6)$$

where α is the firing angle, μ is the commutation angle and I_1 is the rms fundamental current with no overlap.

In addition to the characteristic harmonics, harmonics of uncharacteristic orders are also produced. These harmonics are caused by unbalance or variation in voltages and line impedances, by unequal spaced firing angles of the 3-phase thyristors and also by the interaction of characteristic harmonics and fundamental currents in nonlinear elements of the power systems. The harmonics of low uncharacteristic orders are normally much smaller than the corresponding adjacent characteristic harmonics.

Theoretically, a 12-pulse converter does not produce 5-th, 7-th, 17-th and 19-th harmonics, but due to unbalances, some will be present. Ref. [47] recommends the assumption that these uncharacteristic harmonics are approximately 15 to 25% of those computed for a 6-pulse converter. For a 6-pulse converter, if the firing angles of thyristors are delayed or advanced by 1°, the 2nd, 3rd and 4-th harmonics are each approximately 1 - 2% of the fundamental current [6].

Medium Size Converters

These types of converters are mostly used for motor speed drives or controls. Earlier applications were developed around the converter-fed dc drives, which still hold the main share of the market. Ref. [48] presented a technique for calculating the line current and voltage harmonics generated by a thyristor dc motor drive with a practical value of converter commutation reactance and finite (relatively small) value of motor load inductance on the dc side of the converter. However, the emphasis is now shifting towards the use of inverters for controlling induction or synchronous machines (ac motor drives). The most common types of ac drives for induction motors are ac voltage controller, variable-voltage variable-frequency pulse width modulation drive, variable-voltage variable frequency square-wave drive, controlled current inverter (variable-current variable frequency) drive and cycloconverter drive; while the drives for synchronous machines include voltage-fed inverter and current-fed inverter (load commutated inverter). The harmonic currents injected by each of these drives which depend on the motor speed and the type of control

arrangement used, are well documented in Ref. [49].

Low Power Converters

Converters with low power ratings are mainly used in home and office appliances such as TV receivers [50], stereo sets, microwaves and personal computers. Due to their low power ratings, these converters generate relatively small harmonic currents. However, the harmonics will become significant when large numbers of these individual units are simultaneously active. The harmonic contribution of battery chargers is also included in this category. Battery chargers are considered as major sources of harmonics when the use of electric vehicles becomes generally accepted [51].

2.1.1.2 Other Harmonic Sources

Prior to the development of static power converters, the sources of harmonics were primarily associated with electric machines and transformers. Modern transformers and rotating machines under normal steady-state operating conditions do not cause significant distortion in the network. However, during transient disturbances and when operating outside their normal state range, they can considerably increase their harmonic contribution. Other nonlinear loads that produce harmonics and need to be considered are arcing devices (arc furnaces, arc welder and arc lighting), fluorescent lamps and static VAR compensators.

Transformers

Due to the nonlinearity in the transformer magnetization curve (magnetic saturation problem), the magnetizing current produced with a sinusoidal supply voltage will not be sinusoidal. The harmonic content of the magnetizing current will increase substantially because of symmetrical overexcitation or overvoltage saturation. Such distortion contains mainly triple harmonics, particularly the third harmonic. The fifth and seventh harmonic

components may also be large enough to produce visible distortion and can not be ignored.

The transformer is also known to generate an inrush current when it is re-energized after being switched off. Because of the residual flux left in the core, the transformer may be driven to extreme saturation and will thus produce excessive ampere-turns in the core. This effect gives rise to magnetizing currents of up to 5 - 10 times the rated current [4].

Electric Machines

Electric machines usually generate odd harmonics because of the rectangular m.m.f. (magnetomotive force) and flux distribution produced in a full-pitched polyphase winding. If the machine has m slots per pole, the harmonics of orders $(2m \pm 1)$ will be generated. For induction motors with a rotor slip s, a harmonic of order h in the rotor m.m.f. induces an e.m.f. (electromotive force) in the stator at a frequency equal to $(h - s(h \pm 1))$ times the fundamental frequency [52].

Harmonics can also occur as a result of an electrically unbalanced rotor winding. In such a case, both positive and negative phase sequence currents will flow in the rotor, creating forward and backward rotating fields. The harmonic frequencies of stator e.m.f. induced by these fields are (1 - 2s) times the fundamental frequency. Electric machines with magnetic reluctance variations caused by stator and rotor slots also generate harmonics, but these harmonics are not significant.

Arcing Devices

The most common arcing devices are arc furnaces, arc welders, mercury arc lighting and fluorescent lamps. For arc furnaces and welders, a combination of arc ignition delays and the highly nonlinear arc voltage-current characteristics introduce harmonics. The harmonic currents produced by these loads are of all harmonic orders (h = 2, 3, 4, 5, ..., 9, 10, ..), with the average harmonic levels of about 5% (of the fundamental) for the 3rd harmonic, 4.5% for the 2nd or 5-th harmonic, 2.8% for the 4-th harmonic, 1.7% for the 6-th or 7-th harmonic and about 1% for the 8-th, 9-th or 10-th harmonic [4]. The magnitudes

of these harmonics vary randomly with time due to the sudden changes of arc length, especially during the melting phase.

Arc lighting and fluorescent lamps have the same nonlinear behavior, i.e., the voltage builds up across a gap until the gases in the gap ionize, preventing further increase in the voltage. This causes the voltage across the gap to resemble a square-wave. The current contains mainly the third and fifth harmonics with magnitudes of 21% and 7% of the fundamental component, respectively.

Static VAR Compensators

Because of their ability to continuously adjust the reactive power, fast response, high efficiency and low maintenance, static VAR compensators are mainly used for improving voltage regulation, improving power system stability, compensating power factor and correcting phase unbalance [5]. The most commonly used compensators are thyristor-controlled reactors (TCR) and thyristor-switched capacitors (TSC), which generate a considerable amount of harmonic distortion. The magnitudes of these harmonics depend on the delay angles of the SCR's. The dominant harmonic currents generated by TCR are the 3rd and 5-th harmonics with maximum amplitudes of 13.8% and 5% of the fundamental components, respectively.

2.1.2 System Component Models

To analyze harmonics using analytical and computer methods, it is required to represent all power system components by their equivalent circuits. Most linear and passive components can be represented by equivalent impedances. Nonlinear or harmonic-producing loads are modeled as harmonic voltage or current sources with/without equivalent impedances depending on the accuracy needed in the computation. The equivalent circuits are generally frequency-dependent. Table 2.1 shows the commonly used equivalent circuits for most of the system components.

Table 2.1 System Component Models

Nonlinear Load	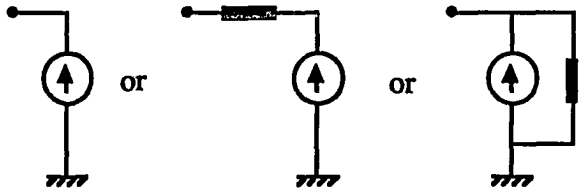
Transformer	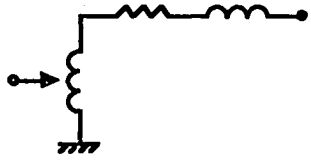
Induction or Synchronous Machine	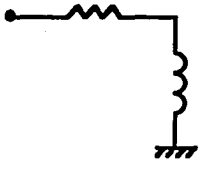
Line/Cable	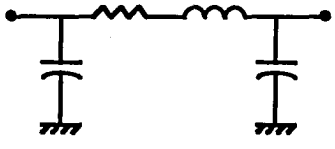
Linear Load	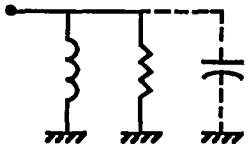
Inductor, Capacitor	
Equivalent of Remaining Network	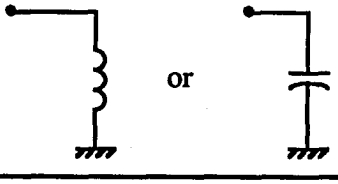

Nonlinear Loads

Static power converters are the main nonlinear (harmonic-producing) loads in power distribution systems. They can be grouped into line-commutated and self-commutated converters. Line-commutated converters are represented as ideal constant harmonic current sources at their characteristic harmonic frequencies. For the ideal case of instantaneous commutation between the conducting elements (no overlap angle), the ac side harmonic orders and their magnitudes are given by eqns (2.1) - (2.4). When the commutation and firing angles are taken into account, the harmonic current magnitudes are given by eqns (2.5) - (2.6).

Self-commutated converters differ from line-commutated devices in that they employ additional circuit elements for forced commutation. As a harmonic source, the converter module is represented by a current source at a characteristic harmonic frequency behind a series or parallel impedance as shown in Fig. 2.1(a) or 2.1(b). The impedance may consist of a pure inductance, R-L in series or R-L in parallel.

When it is necessary to obtain more accurate representation of the nonlinear devices under a variety of circuit conditions, a hybrid model consisting of a transient simulation of the device characteristics and a steady-state solution of the linear network is usually required [28,29]. In this modeling method, the steady-state solution is determined iteratively by incorporating a series of equations or a time-domain solution that accurately represents the behavior of the nonlinear device in the transient simulation. The nonlinear devices are represented as variable current sources in the steady-state solution. The hybrid approach has been successfully applied to the harmonic power flow technique developed by Ref. [21].

The arc furnace and most other arcing devices can be modeled as harmonic current sources in parallel with inductive reactances. The inductance is measured with the arcing element shorted. Due to the random nature of arc currents, the magnitudes of harmonic currents must be approximated by the average values in order to be incorporated in steady-

state harmonic analysis. For most other nonlinear loads, ideal harmonic current source models are generally adequate for a wide range of circuit conditions when the voltage distortion is not greater than 10%. Transformers and electric machines are also known as harmonic producers. However, the harmonics they produce during steady-state operating conditions are relatively small compared to those produced by solid-state power converters. Therefore, these harmonics are ignored, and transformers and electric machines are treated as linear components.

Transformers

Transformers are usually represented as equivalent leakage impedances (R-L in series), with the shunt magnetizing impedances ignored. The leakage impedance is a function of frequency. A typical transformer impedance variation curve is given in Ref. [30]. A good approximation is to assume that the transformer's X/R ratio remains constant as frequency increases. A phase shift transformer model is needed to represent the Y-Δ transformer connection.

Induction Machines

The exact equivalent circuit for a 3-phase induction machine is shown in Fig. 2.2(a). In many cases, including harmonic analysis, the magnetizing inductance L_m is ignored, leaving a simple approximate circuit as shown in Fig. 2.2(b).

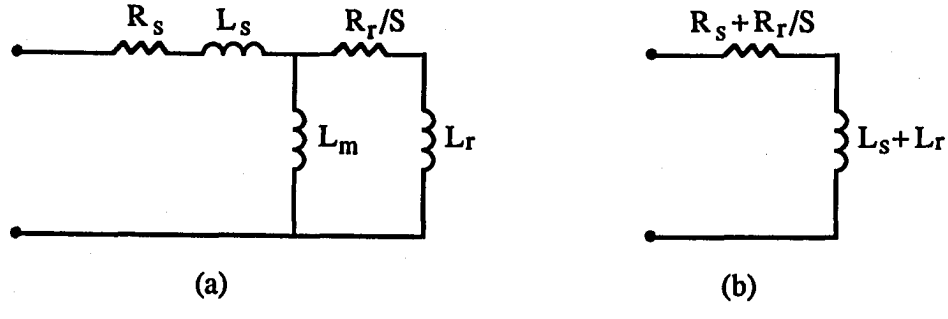

Fig. 2.2 Equivalent Circuit of Induction Motor: (a) Exact, and (b) Approximate

When the motor rotates at a speed close to its synchronous speed, the slip at the h-th harmonic frequency is $S = 1 \pm 1/h$. The slip approaches unity as h increases. For this reason, it is suggested in Ref. [17] that, as a first approximation, induction motors can be modeled by their equivalent locked rotor elements. Furthermore, the reactive term is much larger than the series resistance so that the model can be reduced to a pure inductive reactance (negative-sequence reactance).

Synchronous Generators

The effective inductance encountered by the harmonic currents is the negative-sequence inductance, which is the average of the direct-axis and quadrature-axis subtransient inductances [53]. If the equivalent resistances representing the core and damper winding losses are neglected, the generator can be satisfactorily represented by its negative-sequence reactance in series with the stator winding ac resistance.

Lines and Cables

For analysis of low frequency harmonics (up to 17-th harmonics), relatively short overhead lines and cables are represented as nominal pi-equivalent circuits connected in cascade. For higher harmonic frequencies, the lines and cables are represented as the exact pi-equivalent circuits.

Linear Loads

As suggested in Ref. [17], loads which are not well defined can be represented as a shunt resistance, R, in parallel with a shunt inductance, L, or capacitance, C, given by,

$$R = \frac{V^2}{P}, \qquad L = \frac{V^2}{\omega Q}, \qquad C = \frac{Q}{V^2 \omega}, \tag{2.7}$$

where $\omega = 2\pi f$, f is the fundamental frequency, V is the line to line voltage, and P and Q are the 3-phase active and reactive power of the load, respectively.

If the linear loads are distributed, they may be treated as equivalent lumped loads divided at the two ends of the line section over which they are distributed.

Capacitors and Inductors

Capacitors are usually modeled as pure capacitances with no resistive losses. Inductors are modeled as inductances with or without resistive losses. The reactance of a shunt capacitor is inversely proportional to the frequency, and the reactance of an inductor is directly proportional to the frequency.

Equivalent Circuit for the Remaining Network

In a large power system, it is difficult to include detailed models of all network components. Thus, only system components that are located in the region of interest need to have complete representation for obtaining accurate results. The remaining network, outside the region of interest, is replaced by an appropriate Thevenin equivalent. Ref. [54] suggests that the remaining network connected to an outside bus (defined as a bus on the border of the region of interest) should be represented by the short-circuit negative-sequence reactance at the power frequency times the harmonic order under consideration. However, in some situations, the remaining network may be represented by an equivalent capacitive reactance.

2.2 Harmonic Analysis

Analytical methods and commercially available computer programs for analyzing harmonic propagation and penetration into power systems are discussed in this section.

2.2.1 Harmonic Power Flow

The harmonic power flow technique was introduced in Ref. [14]. In this approach, the conventional Newton-Raphson power flow study is reformulated to permit the inclusion of nonlinear loads. The reformulation is based on the reduction to zero of the

mismatch active power and reactive voltamperes, the unbalanced current at harmonic frequencies, and the mismatch apparent voltamperes. Before including harmonics in the power flow program, it is necessary to know a priori the steady-state voltage - current relationships at nonlinear load buses, from which the Fourier series expansion of the load current is obtained in terms of harmonic load voltage and nonlinear load parameters.

In the harmonic power flow study, it is assumed that the load apparent voltamperes, S, at nonlinear load buses are known. It is also assumed that the type of nonlinearity is known. The other specified (known) quantities are the total active power at all buses except the swing bus, and the total reactive voltamperes at all linear load buses except the swing bus. Bus voltage magnitudes and angles for fundamental and harmonic frequencies are unknown quantities. The additional equations are derived from Kirchhoff's current law for fundamental and harmonic frequencies and the conservation of apparent voltamperes at nonlinear load buses.

The resulting matrix formulation of harmonic power flow is given by [14]

$$\begin{bmatrix} [\Delta W] \\ [\Delta I_1] \\ [\Delta I_5] \\ \cdot \\ \cdot \\ \cdot \end{bmatrix} = \begin{bmatrix} [J_1] & [J_5] & [J_7] & \cdot & \cdot & [0] \\ [YG_1^1] & [YG_1^5] & [YG_1^7] & \cdot & \cdot & [H_1] \\ [YG_5^1] & [YG_5^5] & [YG_5^7] & \cdot & \cdot & [H_5] \\ \cdot & \cdot & \cdot & \cdot & \cdot & \cdot \\ \cdot & \cdot & \cdot & \cdot & \cdot & \cdot \\ \cdot & \cdot & \cdot & \cdot & \cdot & \cdot \end{bmatrix} \begin{bmatrix} [\Delta V_1] \\ [\Delta V_5] \\ [\Delta V_7] \\ \cdot \\ \cdot \\ [\Delta \xi] \end{bmatrix} \tag{2.8}$$

where:

$[\Delta W]$ = mismatch active power and reactive voltamperes at all buses,

$[\Delta I_1]$ = mismatch fundamental real and imaginary currents at nonlinear load buses,

$[\Delta I_k]$ = mismatch k-th harmonic real and imaginary currents at all buses ($k \neq 1$),

$[\Delta V_k]$ = fundamental and harmonic voltage magnitudes and angles at all buses ($k \geq 1$),

$[\Delta \xi]$ = state variable mismatch for each nonlinear load,

$[J_1]$ = conventional power flow study Jacobian matrix,

$[J_k]$ = k-th harmonic Jacobian matrix,

$[H_k]$ = partial derivatives of nonsinusoidal real and imaginary load currents with respect to firing angles and commutation resistances,

$$\left[YG_j^k\right]=\begin{cases}\left[Y_k^k\right]+\left[G_k^k\right], & k=j\\ \left[G_j^k\right], & k\neq j\end{cases} \tag{2.9}$$

$\left[Y_k^k\right]$ = partial derivatives of injected k-th harmonic currents with respect to k-th harmonic voltages as derived from the system admittance matrix, and

$\left[G_j^k\right]$ = partial derivatives of the k-th harmonic load currents with respect to the j-th harmonic supply voltages as determined by the nonlinear load characteristics.

In the implementation and practical application shown in Ref. [14], it is noted that the convergence for harmonic power flow studies is slower than for conventional (fundamental) power flow studies, because initialization of the harmonic signals is difficult and often unpredictable. Due to this limitation, the harmonic power flow algorithm is limited to balanced and relatively small systems.

A computer program called HARMFLO [15,16], which is based on the technique described above, is available from the EPRI Software Center. The program has some restrictions, i.e., no more than 30 buses can be modeled in the current version of the program and it is recommended that a frequency range limited between 60 and 1140 Hz (19-th harmonic) be used.

2.2.2 Current Injection Method

An alternative approach to predict harmonic penetration into a power network is based on the harmonic current injection response of the network. The nonlinear loads are modeled as harmonic current sources with or without load impedances. These current

harmonics are functions of their fundamental load currents (both magnitude and phase angle). Based on the size of power network, the calculation methods can be divided into manual method and computer method.

2.2.2.1 Manual Method

The manual method is basically limited to very simple circuit configurations consisting of only one or two loops. Localized harmonic studies for the balanced circuit case can be easily handled by this method. Fig. 2.3 shows a simple circuit representing industrial loads with a compensating (power factor) capacitor connected to a substation transformer.

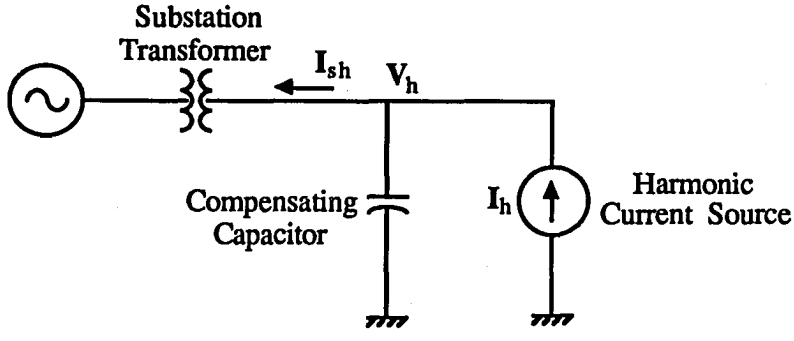

Fig. 2.3 Circuit Configuration for Manual Method

The total source impedance ($Z_S = R + j\,\omega L$), which is generally dominated by the transformer impedance, together with the compensating capacitor (C) determine the frequency response of the system. The resonant frequency (with R neglected) is given by

$$f_r = \frac{1}{2\pi\sqrt{LC}}. \qquad (2.10)$$

The resonant frequency should not be near the frequency of the injected harmonic currents.

The h-th harmonic voltage at the harmonic source terminal is

$$V_h = I_h \frac{R + j\,\omega_h L}{(1 - \omega_h^2 LC) + j\,\omega_h R\,C}, \tag{2.11}$$

where $\omega_h = 2\,\pi f\,h$, I_h is the h-th harmonic current produced by the harmonic source, and the h-th harmonic current injected into the utility system is

$$I_{sh} = V_h \frac{1}{R + j\,\omega_h L}. \tag{2.12}$$

The total harmonic distortion at the source terminal is computed as

$$THD = \frac{\sqrt{\sum_{h>1} |V_h|^2}}{|V_1|}. \tag{2.13}$$

2.2.2.2 Computer Method

The main difference between manual and computer methods is the size of the circuit analyzed and the amount of calculation made. For a large power system such as a radial distribution system with multiple buses and distributed nonlinear loads, the computer method is required for analyzing the harmonic flows. Harmonic analyses for different harmonic frequencies are treated separately, and the results are then combined by superposition.

Consider a balanced and symmetrical n-bus distribution system with harmonic current sources injected at bus i through bus j. The bus harmonic voltages for harmonic order h can be calculated as

$$\left[V_{bus}^h\right] = \left[Z_{bus}^h\right]\left[I_{bus}^h\right] \tag{2.14}$$

where

$\left[V_{bus}^h\right] = \left[V_1^h\, V_2^h \cdots V_n^h\right]^T$ = (n × 1) bus harmonic voltage vector,

$\left[I_{bus}^h\right] = \left[\cdots I_i^h \cdots I_j^h \cdots\right]^T$ = (n × 1) bus harmonic current injection vector,

$$[Z^h_{bus}] = \begin{bmatrix} Z^h_{11} & Z^h_{12} & \cdots & Z^h_{1n} \\ Z^h_{21} & Z^h_{22} & \cdots & Z^h_{2n} \\ \vdots & \vdots & \cdots & \vdots \\ \vdots & \vdots & \cdots & \vdots \\ Z^h_{n1} & Z^h_{n2} & \cdots & Z^h_{nn} \end{bmatrix} = (n \times n) \text{ bus impedance matrix,} \quad (2.15)$$

and superscript T indicates transposition. A technique for constructing the bus impedance matrix, $[Z^h_{bus}]$, is explained in Ref. [55].

The h-th harmonic line current flowing from bus m to bus k and the h-th harmonic load current at bus m are respectively given by

$$I^h_{mk} = \frac{V^h_m - V^h_k}{z^h_{mk}} \quad (2.16)$$

and

$$I^h_{Lm} = \frac{V^h_m}{z^h_{Lm}}, \quad (2.17)$$

where z^h_{mk} and z^h_{Lm} are the line impedance between bus m and k and the load impedance at bus m for the h-th harmonic frequency, respectively.

Note that the h-th harmonic bus voltages are dependent on both the magnitudes and phase angles of the harmonic current sources of the same harmonic order. The phase angles can be found from the phase relationships between the harmonic currents and their corresponding fundamental currents, along with the phase relationships between the fundamental currents at the harmonic source buses.

V-HARM

A computer program based on the above equations (2.14) - (2.15), i.e., using the bus impedance matrix and harmonic current injections, is now commercially available. The program is called V-HARM [20], which can be used in an IBM personal computer (PC)

XT, AT, or other IBM-compatible computers. It also takes full advantage of graphics capabilities of the PC. Graphic-oriented output options include the frequency scan plots, 3D-plots, R-X plots, harmonic spectrums, and waveform reconstruction. The program is a powerful, interactive simulation tool for power system harmonic analysis. It can determine the frequency response characteristics of a power system as well as the calculation of harmonic levels throughout the system caused by known harmonic sources. Potential harmonic problems can be identified and solved before they cause equipment failures or customer complaints and without extensive field testing and measurement procedures.

The V-HARM program supports a complete system representation of all types of power system equipment and harmonic-producing devices, including unbalances in the circuit and loads, frequency dependence of device characteristics, and multiple harmonic sources. A complete three-phase circuit model including mutual coupling between phases, or a simplified single-phase model can be used, depending on the application.

The V-HARM Solution Module has been structured to efficiently utilize memory on the PC. The program uses dynamic memory allocation, virtual memory and sparse matrix techniques. This permits the representation of systems with up to 500 nodes. Systems larger than this are handled by using extended memory and/or the hard disk as virtual memory devices. The limiting factors for the system size are the size of the available memory, the simulation times and the round off error accumulation.

Q'HARM

Formulation of a new and computationally fast harmonic power flow program for small power systems, the Q'HARM, is developed and discussed in Ref. [21]. The computer program employs basically the fundamental real and reactive power balance equations for updating the fundamental bus voltages, and the harmonic current balance equations (with the bus impedance matrix) for updating the harmonic bus voltages. Because of its modular structure, the Q'HARM can easily be used to handle systems with

varying structures, such as the electric train power distribution systems. Two types of harmonic-producing loads, the line commutated six-pulse bridge rectifier and the gaseous discharge lighting load, are accurately modeled in this program. The effect of filters is included in the formulation and the calculation of telephone influence indices at any point along the transmission line is performed.

The Q'HARM program consists of ten modules which are executed sequentially. These modules are Input Data Module, Transmission Line Module, Fundamental Power Flow Module, Y_{bus} Module, Z_{bus} Module, Nonlinear Resistor Module, Six-Pulse Line Commutated Converter Module, Harmonic Power Flow Module, Output Data Module, and Communications Interference Module.

2.3 Harmonic Measurement and Instrumentation

Two main purposes for performing harmonic measurements are to verify the simulation model being used and to provide background information on system harmonic sources. The measurements are also used for active control of harmonic filtering devices. With harmonic measurement as a complement of the harmonic analysis procedure, the overall objectives of the integrated measurement/simulation procedure are to characterize and correct an existing harmonic problem, to estimate voltage distortion and/or harmonic current magnitudes resulting from new system additions and to determine background harmonic levels on the system in general for different system conditions.

The instrumentation components which are required to accomplish harmonic measurements are voltage and current transducers, signal conditioning equipment, and signal analysis and monitoring equipment [22,23].

Voltage and Current Transducers are required to convert the system voltage and current to the acceptable levels for input to the signal conditioning equipment. These transducers can be either permanently installed devices or specially designed transducers. Permanently connected voltage and current transducers, such as capacitor dividers or

magnetic potential transformers and current transformers, are convenient when they are available. However, the disadvantage is that their frequency response characteristics are usually unknown.

Signal conditioning equipment involves conversion of the signals being measured from the output levels of the transducers to levels appropriate for the input to the processing and monitoring equipment. Filtering can also be employed as part of the signal conditioning to improve the dynamic range of the measurement system.

Signal analysis and monitoring equipment may include a spectrum analyzer, an oscilloscope, a multimeter, and a tape deck, depending on the field test objectives. An oscilloscope and a multimeter are recommended for calibration of equipment and monitoring of the actual waveforms. The spectrum analyzer is required to resolve the measured waveform into its frequency components. The Fast Fourier Transform (FFT) - based spectrum analyzers are the most well known and convenient for real-time harmonic analysis. Most FFT-based analyzers provide signal-averaging capability that enhances the measurement of low-power signals in the presence of noise. Microprocessor-based digital harmonic analyzers have been recently built, tested and discussed in Refs [24,25]. A tape deck is needed if the tests require simultaneous measurement of multiple signals. Three-phase voltages and currents may be required for some calculations such as sequence quantities and unbalances.

2.4 Harmonic Reduction and Control

To limit the harmonic distortion in a power system to an acceptable value, reduction and control may be required either at the harmonic source, or in the power network. The harmonic reduction methods can be classified as harmonic cancellation or harmonic filtering. Several other methods of harmonic control are magnetic flux compensation, harmonic current injection, dc ripple reinjection and pulse width modulation. Although harmonic reduction is the subject of Chapters 4 and 5, an overview will be given here.

2.4.1 Harmonic Cancellation

Harmonic cancellation involves the use of either transformers or specialized magnetics to phase-shift multiple converters in order to obtain cancellation of certain harmonics at the harmonic source. Essentially, harmonic control takes place through the cancellation of certain harmonics by increasing the converter pulse number, p. The relationship between pulse number and harmonic order is given in eqn (2.1). The equation indicates that an increased pulse number corresponds to an increased frequency of the lowest harmonic order produced. As an example, a 6-pulse converter generates harmonics of order 5, 7, 11, 13, 17, 19, 23, 25, ... on the ac side. A 12-pulse configuration, which is constructed by cascading two 6-pulse converters, one with Y-Y and the other with Y-Δ connected transformer banks, generates harmonics of order 11, 13, 23, 25, ..., as a result of cancelling harmonics of order 5, 7, 17, 19, ... In practice, the cancellation is not perfect. The percentage cancellation for the 5-th and 7-th harmonics is on the order of 75 - 85% of the full rated harmonics [3]. This type of cancellation is economical for increasing the pulse number up to 12-pulse, but it may become uneconomical for higher pulse numbers (beyond 12-pulse).

The advantage of this method is that harmonic cancellation takes place independently of the power system configuration. The disadvantages are the increased number of transformers that are used both in service and spares, the increased complexity of transformer connections and the consequent problems of insulation.

2.4.2 Harmonic Filtering

There are two approaches to passive harmonic filtering in a power system: filtering harmonic sources (which are the nonlinear loads) or filtering the distribution feeders. It is practical to filter the harmonic source when there is only one major source in the system. Source filtering is also applicable for several harmonic sources when their magnitudes and locations are known a priori or can be identified. However, as the number of nonlinear

loads increases and they are widely distributed throughout the network, placing a filter at/near each harmonic source becomes impractical and uneconomical. In this case, filtering the entire distribution feeder regardless of the source of harmonic distortion should be considered.

2.4.2.1 Filtering Harmonic Sources

Depending on how many harmonic frequencies need be filtered, the method is to place a shunt filter or filters (multiple branches in parallel) at/near the harmonic source bus. The shunt filters, which are connected from line to ground, establish low impedance (short circuit) paths to ground for current source harmonics, so that harmonic currents do not enter the system network. The filters also provide all or part of the reactive power consumed by the nonlinear loads, the remainder being supplied by capacitor banks.

The most commonly used shunt filters are RLC series - tuned filters for lower harmonic frequencies and a single high-pass filter for the seventeenth and higher harmonics. The design of filters, including their cost is the subject of Chapter 4. It is discussed in general below.

An important factor to be considered in designing a tuned filter is the frequency-dependent driving point impedance (network impedance) looking into the power network at the source terminal. The harmonic source which is represented as an ideal current source, I_{hs}, is connected to the filter impedance, Z_{hf}, in parallel with the network impedance, Z_{hnet}, as shown in Fig. 2.4.

The harmonic voltage and currents in the network and filter at harmonic order h, respectively, are

$$V_h = \frac{Z_{hf}\, Z_{hnet}\, I_{hs}}{Z_{hf} + Z_{hnet}}, \tag{2.18}$$

$$I_{hnet} = \frac{Z_{hf}\, I_{hs}}{Z_{hf} + Z_{hnet}}, \tag{2.19}$$

$$I_{hf} = \frac{Z_{hnet}\, I_{hs}}{Z_{hf} + Z_{hnet}} . \qquad (2.20)$$

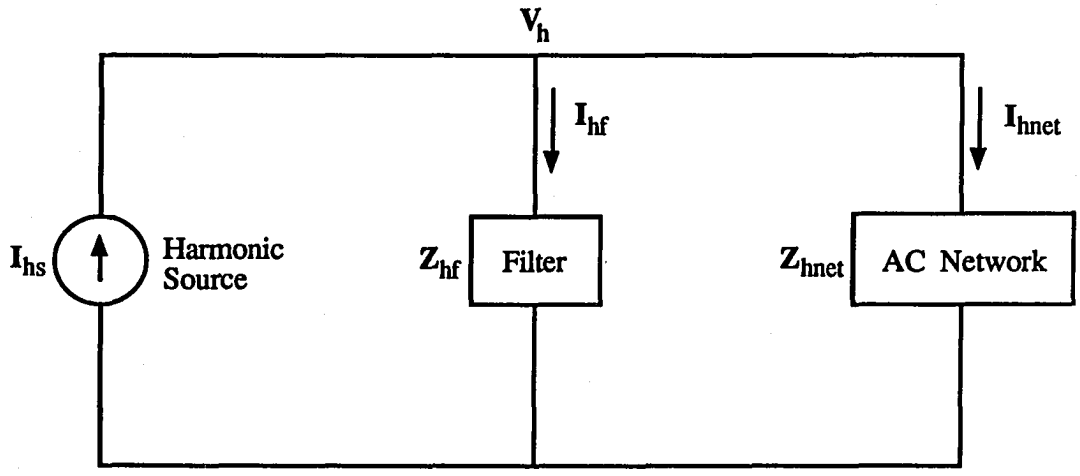

Fig. 2.4 Equivalent Circuit of an AC Power Network with Harmonic Source and Filter

The objective is to select filter components that minimize the harmonic voltage, V_h, in eqn (2.18). The variables in designing the filter are the quality factor (Q) of the inductor and the size of the filter. Thus, V_h, is minimized with respect to the value of Q.

The optimum value of Q is found as [4,6]

$$Q_o = \frac{\cos \phi_m + 1}{2\, \delta_m \sin \phi_m} , \qquad (2.21)$$

and the corresponding minimum harmonic voltage,

$$V_h = \frac{4\, \delta_m\, \omega_n L\, I_{hs}}{\cos \phi_m + 1} , \qquad (2.22)$$

where ϕ_m is the limiting value of network impedance angle, δ_m is the maximum frequency deviation, and ω_n is the tuned angular frequency. The value of ω_n is selected to be below the harmonic frequency by a few percent to prevent parallel resonance with source inductance [27].

The total cost of filter is defined as [4,6] (neglecting the cost of power losses in the resistor),

$$TCOST = U_T + A\ S + \frac{B}{S}, \tag{2.23}$$

where

$$A = \frac{h^2}{h^2 - 1}\left(U_C + \frac{U_L}{h^2}\right),$$

$$B = \frac{h^2}{h^2 - 1}\frac{V_1^2 I_{hf}^2}{h}\left(U_C + U_L\right),$$

$$S = \frac{V_1^2}{X_C - X_L} = \text{filter size [4,27]}, \tag{2.24}$$

V_1 is the fundamental supply voltage, U_T is the total constant cost of the filter branch, and U_C and U_L are the unit costs of capacitor and inductor per kVAR, respectively.

The size of filter for the minimum cost is found by equating the $d\,(TCOST\,)/dS$ to zero:

$$S_{\min} = \sqrt{\frac{B}{A}}, \tag{2.25}$$

and the corresponding minimum cost is

$$TCOST_{\min} = 2\sqrt{A\,B}\ . \tag{2.26}$$

However, if harmonic currents generated by the nonlinear load are not sufficiently serious to suggest filters, an *LC* compensator can be used to reduce harmonic distortion while maintaining a given displacement factor. This subject will be discussed in Chapter 5.

2.4.2.2 Filtering Distribution Feeders

If harmonic sources are too numerous to be individually filtered, the entire feeder may be filtered by placing one filter at each major feeder branch. The technique is discussed in Chapter 4.

2.4.3 Alternative Harmonic Control Methods

Harmonic filtering is not used to cancel harmonics caused by an unbalanced operation of converters or by unbalanced power system parameters. Other harmonic control methods that have been developed to eliminate these harmonics are magnetic flux compensation, harmonic current injection, dc ripple injection and pulse width modulation. These methods can eliminate all harmonics regardless of frequency, but they are complex and expensive.

Magnetic Flux Compensation

This method is based on the principle of magnetic flux compensation in a converter transformer core, which is accomplished by injecting a compensating current into a transformer tertiary winding [56]. A current transformer is used to detect the signal waveform coming from the nonlinear load in the secondary winding. First, a 60 Hz filter removes the fundamental component from the waveform, then the resulting current signal is amplified through a power amplifier and fed into a tertiary winding of the converter transformer in such a way as to oppose the m.m.f. produced by the secondary current harmonics. In this way, harmonic components in the transformer magnetic flux can theoretically be cancelled, which will result in a distortionless waveform of the transformer primary current.

This method has been developed, tested and discussed in Ref. [57]. A specialized power amplifier, which is a switched-mode power amplifier using full bridge configuration, has been designed and built for the experiment.

Harmonic Current Injection

This method is similar to flux compensation. A harmonic current from an external source is added to the converter distorted current waveform. In such a scheme, as originally proposed by [58] and later developed by [59], a triple harmonic from the source is injected in the conducting transformer phases. If the injected current is adjusted such that

it is equal in magnitude but 180° out of phase with the converter current harmonic, then the cancellation takes place.

The advantage of the scheme is that the system impedance is not a part of the design criteria. However, the method suffers from disadvantages: (1) need for a triple harmonic current generator and its synchronization to the supply main frequency, (2) difficulty in adjusting the amplitude and phase of the sinusoidal injected current to suit each particular operating condition, and (3) inability to nullify more than one harmonic order to any operating point. The other disadvantages are poor efficiency and applicability only to rectifiers operating with 0° delay.

DC Ripple Injection

This method is an alternative method of current injection. Instead of using an external harmonic source, a square-wave current is fed from the rectifier dc output to the converter transformer through a feedback converter [60]. The feedback converter is connected to the secondary windings of the converter transformer by two additional single-phase transformers and blocking capacitors. With phase and frequency adjustment of the injected current, a 6-pulse rectifier configuration can be converted into a 12-pulse converter system from the point of view of ac and dc system harmonics.

Pulse Width Modulation

This technique is applicable only to self-commutated converters and has been successfully applied in variable speed ac drives [61]. It involves notching of the ac output voltage waveform to reduce or eliminate particular harmonic components. Harmonic control can be obtained by adjusting the widths of the notches. Theoretically, all harmonics up to an arbitrary order can be eliminated. However, in practice, this method is limited by the additional switching losses induced by the number of notches required in one cycle.

CHAPTER 3

HARMONIC SOURCE MONITORING AND IDENTIFICATION USING NEURAL NETWORKS

Before considering the problem of reducing harmonics, the location and type of harmonic sources injected into a power system must be either known a priori or found by measurements. However, harmonic measurements need specialized instruments which are only installed at few buses or lines. State estimation using neural networks is a method of minimizing instrumentation requirements.

Static state estimation of electrical networks is presently used in power systems to extract accurate estimates of fundamental frequency voltages and power flows from redundant, noisy measurements. State estimation is also used to find electrical quantities at uninstrumented buses [62,63]. The same technique can be extended to the measurement of non-fundamental frequency behavior. In power network harmonic analysis, state estimation has been used in identifying harmonic current sources, which are nonlinear loads that may distort load currents beyond an acceptable value [26]. Although the technique of [26] is successful, the method outlined requires a large number of harmonic detectors to be placed throughout the network if harmonic sources are to be monitored continuously. It would be desirable to estimate harmonic sources using state estimation and relatively few permanently instrumented buses. Such estimates would be useful in designing optimum filters to minimize feeder voltage harmonic distortion [45], or LC compensator to minimize local harmonic distortion [46].

What is required is a source of initial estimates, or pseudomeasurements, to substitute for permanent harmonic instrumentation. In general, a network of n unknown complex states requires at least n complex (magnitude and phase angle) measurements to compute the unknowns, and (n+1) measurements to produce an improved estimate of the unknown states. In fundamental frequency state estimation, pseudomeasurements based on a variety of sources are used to get the necessary number of measurements or to increase

redundancy. For harmonic state estimation, pseudomeasurements are not generally available because harmonic sources are variable and difficult to measure directly. The expedient of using known voltage regulator values or known generation schedules in place of actual measurements, as is done in fundamental frequency estimation, is not possible for harmonics. This study explores the use of neural networks to supply pseudomeasurements for harmonic state estimation.

Neural network computing was developed as a method of using a large number of simple parallel processors to recognize preprogrammed, or "learned", patterns. This approach can be adapted to recognizing learned patterns of behavior in electrical networks where exact functional relationships are not easily defined. A neural network was used in Ref. [64] to associate patterns of prefault voltage angles and immediate postfault accelerating power with the critical clearing time for a faulted line. In another paper [65], a neural network strategy was used to recognize current waveforms associated with incipient (high impedance) faults on distribution feeders. Recently, a two-stage neural network approach is proposed in Ref. [66] for real-time control of multi-tap capacitors installed on a distribution system with a nonconforming load profile. In these papers, neural net computing was used because the nature of the input-output functional relationship was either not well defined or not easily solved. The neural network was able to compute the answer quickly by using associations "learned" from previous experience, gained either from time-domain simulation or practical experience.

In the case at hand, the neural network must "learn" to associate the available power network data patterns with patterns of harmonic source behavior. This behavior can be learned from system operating data and data obtained from temporary harmonic source monitors at known sources. The neural network will then estimate harmonic sources based on experience in the same way an experienced operator infers pseudomeasurements from available data for conventional state estimation.

In this chapter [44], neural networks to make initial estimates of harmonic sources

will be discussed first. The initial estimates will be used as pseudomeasurements. Then a state estimator to use redundant data from measurements and pseudomeasurements will be discussed. Finally, the results of a network simulation will be presented.

3.1 Neural Network

Neural network computing is distinguished from conventional pattern recognition by its capability to map complex and highly nonlinear input-output patterns. It can be used to classify patterns by selecting the output which best represents an unfamiliar (unknown) input pattern in cases where an exact input-output functional relationship is not easily defined. The input and output patterns may be binary or analog signals.

A neural network is composed of nonlinear computational elements (processing units) operating in parallel. The processing elements are connected by links with weights that are selected to produce the desired associations. Several types of neural network models are discussed in Refs [67-69]. For example, the original Rosenblatt model [67] was a single-layer perceptron which had either binary or analog inputs. However, a multi-layer, feedforward machine of the type developed by Rumelhart et. al. [69] will be used in this study. The multi-layer perceptron can be trained as desired by using analytical functions for the activation of the network nodes ("neurons") and by applying a backward error propagation algorithm to update the interconnecting weights and thresholds until proper recognition capability had been attained.

A typical two-layer feedforward neural network, taken from Refs [68,69], is shown in Fig. 3.1. The nodes are processing units which receive input from their lower side and deliver output on the upper side. A set of input signals, comprising an input pattern, is applied to the input. The pattern is transmitted to the input of the hidden layer through the weighted network connections. The weighted pattern is received by the hidden layer units, where the signals are combined in an activation function. Adopting the notation of [69], the activation or total input for a unit in layer j is called net_j :

$$net_j = \sum_i w_{ji}\, o_i \tag{3.1}$$

where w_{ji} is the weight of the connection to unit i in the input, and o_i is the output of unit i.

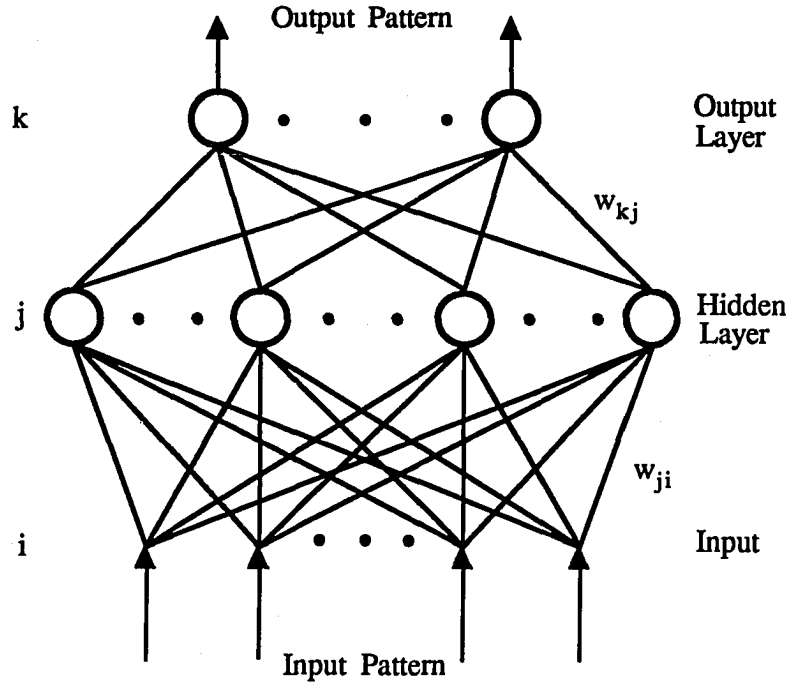

Fig. 3.1 Two-Layer Feedforward Neural Network

The output of unit j is then $f_j(net_j)$. The activation function f is commonly chosen to be the signum in order to resemble the two-state output of biological neurons which originally inspired the network. If the signum is chosen, o_j is determined by a threshold θ_j, as

$$o_j = f_j(net_j) \tag{3.2}$$

where:

$$f_j(net_j) = 1 \quad \text{if} \quad net_j \geq \theta_j \quad \text{and}$$

$$f_j(net_j) = 0 \quad \text{if} \quad net_j < \theta_j . \tag{3.3}$$

The outputs of the hidden layer units are then transmitted to the inputs of the output layer units through another weighted network.

The neural network is thus a pattern associator or classifier, receiving patterns directly from data at the input and delivering output patterns that will give some quantitative information about the system. The problem is to "train" the network by adjusting the weights and thresholds so that the proper prescribed associations will be made. In the case at hand, the information taken in is to be fundamental currents and voltages supplied from around the power network, and any permanently available harmonic measurements. The output pattern is to be the binary representations of harmonic source currents.

The adjustment of the weights and thresholds is done by a training process: a set of input patterns is presented at the input, each along with a desirable, or training, output pattern. Weights are then adjusted to eliminate the total squared error, E_r, which is the sum of squared difference between the set of training outputs for all patterns p, t_{pj}, and the set of actual outputs, o_{pj}:

$$E_r = \sum_p \frac{1}{2} \sum_j (t_{pj} - o_{pj})^2. \tag{3.4}$$

The adjustment could be done by minimizing E_r in a gradient descent if the derivatives of the unit output functions, f'_j, were made continuous. This can be done by replacing the signum function (3.2) with a sigmoid which approximates it [69]:

$$o_{pj} = \frac{1}{1 + e^{-(\sum_i w_{ji} o_{pi} + \theta_j)}}. \tag{3.5}$$

The weights w_{ji} can now be adjusted to minimize E_r for the set of p training patterns by a straightforward application of gradient descent,

$$w_{ji}(ni + 1) = w_{ji}(ni) + \Delta w_{ji}(ni), \tag{3.6}$$

$$\Delta w_{ji}(ni) = \eta \, \delta_{pj} \, o_{pi}, \tag{3.7}$$

where ni is the iteration number, η is the learning rate and

$$\delta_{pj} = (t_{pj} - o_{pj})\, o_{pj}\, (1 - o_{pj}). \tag{3.8}$$

If the unit j is in a hidden layer, t_{pj} is not given, so that

$$\delta_{pj} = o_{pj}\, (1 - o_{pj}) \sum_k \delta_{pk} w_{kj}. \tag{3.9}$$

Better convergence can be obtained if a momentum term is added to equation (3.7),

$$\Delta w_{ji}(ni) = \eta\, \delta_{pj}\, o_{pi} + \beta\, \Delta w_{ji}(ni - 1) \tag{3.10}$$

where β is the momentum factor. These equations are referred to as the delta rule, or generalized delta rule [69].

Equations (3.6) to (3.10) are applied repeatedly to minimize E_r. Incorrect local minima can be recognized by failure to converge to the desired output pattern during the training process. In this case, the gradient descent is started over again using new initial values for w_{ji}. Threshold values, θ_j, are found as if they are weights w_{jk}, where unit k has a constant output o_k equal to 1. The learning rate, η, and the momentum factor, β, in eqn (3.10), are between 0.0 and 1.0, to be determined by experience.

The inputs to the neural network are analog (real numbers). The output is an approximation to binary because of the nature of the sigmoid function. Therefore, output values above 0.5 are interpreted as 1, values below 0.5 as 0. For training, outputs of 1 will be presented as 0.9, and outputs of 0 as 0.1, following the procedure of [69].

There are few definitive rules to follow in selecting a neural network configuration for a given application. It is suggested in Ref. [68] that, for feedforward nets with continuous real inputs and discrete outputs, a two-layer network is sufficient to classify inputs that are limited to convex polygon decision regions. Three-layer nets can classify arbitrarily shaped decision regions. However, there may be no way to know, a priori, the shape of decision boundaries. In fact, if they were known, an exact functional relationship between input and output could be established and the neural net might be unnecessary.

Similar difficulties exist in predicting the total number of hidden nodes required. Clearly the number must be large enough not to restrict the range of output patterns, but too many nodes will require more weights than can be reliably estimated from the available training data. Ref.[68] suggests that patterns similar to analog to digital coding can be done by a net where the number of hidden nodes corresponds to the number of bits. Ref. [68] also interprets a Kolmogorov theorem as suggesting N(2N+1) nodes for a network with a single analog output (where N is the number of analog input variables), but this number is unrealistically high.

3.2 Harmonic State Estimation

The methods of state estimation in power networks have been extensively documented in papers like [62,63]. A practical harmonic state estimation method is proposed and field tested in [26]. Since the purpose of this study is to explore the use of neural networks in conjunction with state estimation, not to apply new estimation methods, a straightforward linear estimation method will be used. This assumes that complex harmonic currents, rather than the more easily measurable complex powers, are the measured and unknown quantities.

If the harmonic impedance of the system is known, current measurements at any harmonic order h may be expressed as a linear combination of bus injected h-th harmonic currents and measurement noise,

$$i_{hm} = A_h \; i_h + s_h \tag{3.11}$$

where i_{hm} is the vector of m current measurements and pseudomeasurements, i_h is the n non-zero injected bus currents, A_h is an (m × n) measurement matrix and s_h is a measurement noise vector. i_{hm} may contain pseudomeasurements of the currents in i_h.

If i_{hm} is properly chosen and m > n, eqn (3.11) may be "solved" for i_h in the least squares sense [62,63]:

$$i_h = \left(A'_h \, R_h^{-1} \, A_h \right)^{-1} A'_h \, R_h^{-1} \, i_{hm}, \tag{3.12}$$

and the state estimate covariance matrix is

$$P_{i_h} = \left(A'_h \, R_h^{-1} \, A_h \right)^{-1}, \tag{3.13}$$

where the prime denotes transposition, and R_h is the (m × m) noise covariance matrix for s_h, which can be expressed as

$$R_h = E[s_h \, s'_h] \tag{3.14}$$

where E denotes the expectation.

If the measurements are all independent, then R_h is a diagonal matrix with diagonal terms

$$R_{ii} = \sigma_i^2. \tag{3.15}$$

σ_i is the standard deviation of noise which is chosen to reflect the degree of confidence in the i-th measurements. For example, instrumentation may have a standard deviation of about 1% of full scale value, while pseudomeasurements may be expected to have standard deviations in the area of 10% to 70% of their highest value. The diagonal elements of P_{i_h} in eqn (3.13) are the variance of the error between the correct values and the estimated values of the state variables, i_h.

3.3 Simulation Tests

A one-line diagram of the IEEE 14-bus system is given in Fig. 3.2. The system has three generator buses, with linear and nonlinear loads at the other buses. Nonlinear loads are represented as impedance loads for the fundamental frequency and as harmonic current sources for higher harmonic frequencies. It should be noted that the network model for harmonic monitoring and identification may, in general, contain any number of buses with linear loads. The model can then be reduced to preserve only buses with nonlinear loads, with linear portions of the network represented by single bus equivalents.

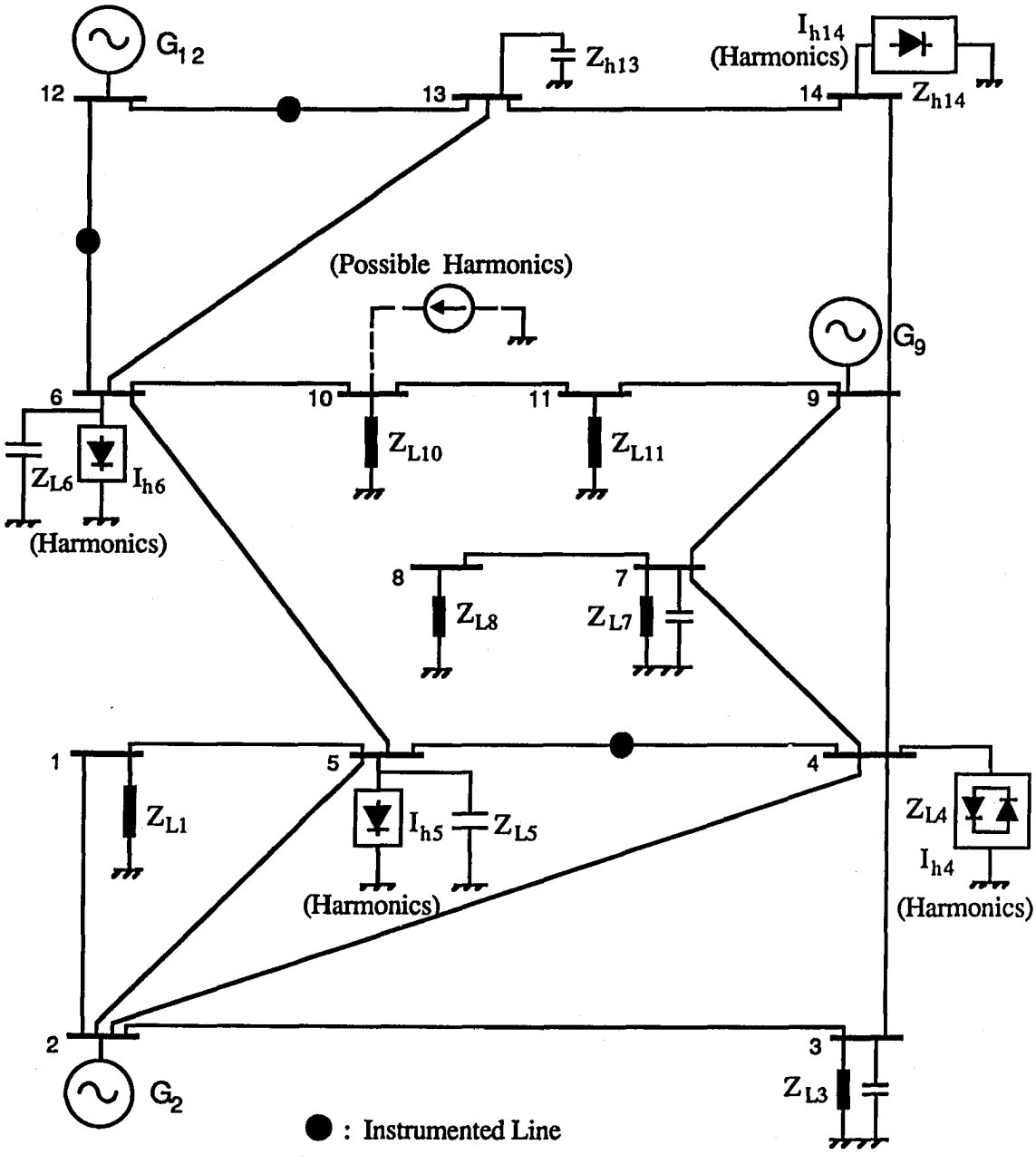

Fig. 3.2 IEEE 14-Bus Test System

In this system, buses 2, 9 and 12 are voltage sources with fundamental voltage at each bus equal to 1.0 $\angle 0°$. Buses 4, 5, 6 and 14 are known to be variable harmonic generators, but they are not permanently instrumented for harmonics although portable instruments can be connected to them to get training data for the neural network. Buses 3, 5, 6, 7 and 13 have fixed capacitors for reactive power control and voltage profile improvement. Bus 10 will also be used as a "possible" source of harmonics in the estimation process. It is assumed that the network is instrumented to provide all fundamental frequency currents and voltages, but only three lines, line 4-5, 12-6 and 12-13, are permanently instrumented for harmonic currents. Line impedances are all assumed equal to (0.02 + j 0.2) pu , and load impedances are given in Table 3.1.

The nonlinear loads at buses 5, 6 and 14 are 3-phase rectifiers simulated by injecting currents (I_{h5}, I_{h6} and I_{h14}) of harmonic order h = 5, 7, 11 and 13. The magnitude of the harmonic currents are 1/h of the corresponding fundamental load current (as in eqn (2.2)), and the phase angles are h times the corresponding fundamental angle with an additional 180° shift for the 5-th and 11-th harmonics (as in eqn (2.3)). The nonlinear load at bus 4 is a 3-phase thyristor-controlled pure resistive load. The generated harmonics are assumed to have same harmonic order as those from the rectifier load. The harmonic currents, I_{h4}, generated by this type of load for h > 1 are

$$I_{h4} = a_h + j\, b_h \tag{3.16}$$

where

$$a_h = \frac{\sqrt{2}\,V}{\pi\, R}\left[\frac{\sin(h+1)\alpha}{(h+1)} - \frac{\sin(h-1)\alpha}{(h-1)}\right]$$

and

$$b_h = \frac{\sqrt{2}\,V}{\pi\, R}\left[\frac{\cos(h+1)\alpha - \cos(h+1)\pi}{(h+1)} - \frac{\cos(h-1)\alpha - \cos(h-1)\pi}{(h-1)}\right],$$

V is the fundamental bus voltage, α is the firing angle and R is the load resistance.

Table 3.1 System Parameters

Bus Data Bus No.	Gen. Voltage [pu]	Source or *Load Impedance Z_L [pu]
1	--	**(2.5 + j 0.8)
2	1.0 ∠0°	**(0.0 + j 0.02)
3	--	***(0.0 - j 40.0)
3	--	**(3.5 + j 1.2)
4	--	**(3.0 + j 0.0) → (6.0 + j 0.0)
5	--	***(0.0 - j 40.0)
5	--	**(2.0 + j 0.5) → (4.0 + j 1.0)
6	--	***(0.0 - j 10.0)
6	--	**(2.25 + j 0.35) → (4.5 + j 0.7)
7	--	***(0.0 - j 30.0)
7	--	**(4.0 + j 1.4)
8	--	**(5.0 + j 0.0)
9	1.0 ∠0°	**(0.0 + j 0.02)
10	--	**(3.0 + j 0.6)
11	--	**(3.7 + j 0.9)
12	1.0 ∠0°	**(0.0 + j 0.02)
13	--	***(0.0 - j 30.0)
14	--	**(3.2 + j 0.6) → (6.4 + j 1.2)

* Load impedance for fundamental frequency only

** Harmonic inductive reactance is h X, where h is the harmonic order

*** Harmonic capacitive reactance is - X_C/h

3.3.1 Neural Network Training Process

A feature encountered in applying neural networks to estimating harmonic current sources was the separability of input-output pairs. When harmonic source measurements (which are neural network outputs) were paired with input measurements (which consist of fundamental load currents and bus voltages at all nonlinear load buses as well as available permanent harmonic line measurements), it was found that each quantity in the output (real

and imaginary parts of each harmonic) was relatively independent. This would be expected for harmonic sources with varying firing angles and/or magnitudes. The output corresponding to a particular harmonic source would be sensitive only to a particular subset of the hidden layer. It was therefore advantageous to divide the neural network into separate networks for each known harmonic source. These can be further divided into two separate neural networks, representing the real and imaginary parts of the harmonic current source, which also behave independently. This eliminated the need to adjust a large number of weights interconnecting the hidden layer with most of the outputs essentially to zero, which aided in obtaining convergence during the training sessions.

The structured neural network of Fig. 3.3 is divided into multiple parallel networks as mentioned above, all with the same inputs, but each with a single 3-bit binary quantity as output. The 3-bit output (corresponding to eight harmonic current levels) was chosen as a compromise between output precision and keeping the number of training lessons manageable. Several lessons are required for each output level, corresponding to several levels in the other harmonic sources. The input set consists of real numbers representing the real and imaginary parts of fundamental load currents and bus voltages at buses 4, 5, 6 and 14, and the fundamental and harmonic complex currents (corresponding to harmonic order of its output) at the permanent metering points on lines 4-5, 12-6 and 12-13, a total of 28 inputs. The outputs, each from a separate neural network, are 3-bit binary numbers representing respectively real and imaginary parts of the 5-th, 7-th, 11-th and 13-th harmonics injected at buses 4, 5, 6 and 14, and another set of 1-bit binary outputs representing the signs of these quantities, for a total of 64 networks with 32 3-bit and 32 1-bit outputs. In addition to the input and output layer, each network contains a 60 node hidden layer.

The neural networks were trained with a series of 72 input-output pairs for bus 5, bus 6 or bus 14 and 108 input-output pairs for bus 4 that were generated by a network simulation of varying harmonic load conditions on buses 4, 5, 6 and 14, and varying firing

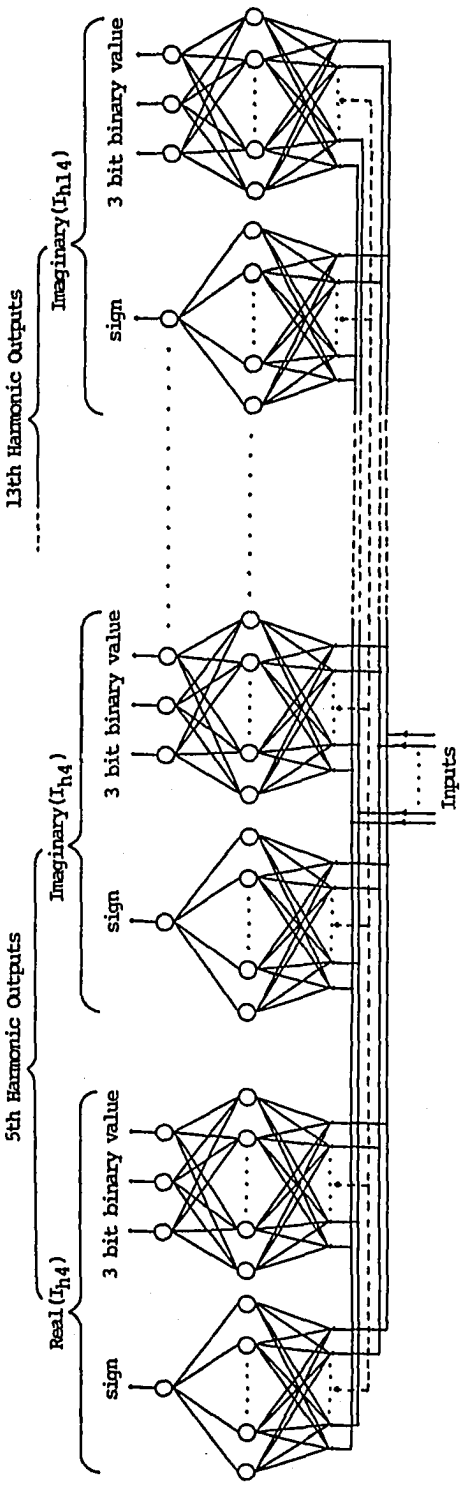

Fig. 3.3 Structured Neural Network

angle, α, of the load at bus 4. The loads were varied to represent all likely load combinations. In practice, training data could be collected by portable recording instruments placed at harmonic sources, which could later be synchronized with appropriate input signals to find input-output training pairs.

In the training process for the neural networks, using equations (3.6) to (3.10), the initial weights and thresholds were randomly selected in the interval [-0.001, +0.001]. After the process converged, the weights and thresholds fell in the interval [-15.0, +15.0]. The other parameters in the training process were the learning rate, η, which is initially chosen to be small (0.2) to prevent overshoot, and the momentum factor, β, which is set to 0.5 (constant). As the algorithm converged, the learning rate was increased to accelerate the convergence. In cases where the algorithm did not converge, or the output converged to values different than the training output, the initial weights and thresholds were altered and the process was started again. Convergence for each training output was obtained in less than 500 iterations of the training set.

3.3.2 Test Results

After the neural networks were trained, the harmonic identification system was tested by four simulations. In the first test, the estimator monitored the harmonic currents that were known to exist at buses 4, 5, 6 and 14. Bus 4 was given an increasing thyristor-controlled load of unknown magnitude with constant firing angle while buses 5, 6 and 14 had constant rectifier loads of unknown magnitudes. For the first three tests, Bus 10 was assumed to be known to have no harmonic current injection. The data for all tests were chosen to fall between the data points used previously in the neural network training process. The neural network supplied pseudomeasurements for each harmonic injection from buses 4, 5, 6 and 14 to the state estimator of equations (3.12) and (3.13), using data from the three harmonic detectors and the known fundamental currents and voltages. The

other sources of measurement data for the vector i_{hm} in eqn (3.12) were the harmonic current detectors on lines 4-5, 12-6 and 12-13. The bottom of Fig. 3.4 is a plot of the magnitudes of fifth harmonic injected model currents, the current magnitudes estimated by the neural networks, and the current magnitudes estimated by the state estimator (using the neural network values as pseudomeasurements) at buses 4, 5, 6 and 14 versus the fifth harmonic model current magnitudes at bus 4. For the state estimation, the real and imaginary parts of the pseudomeasurements were each given a standard deviation $\sigma = 0.01$ pu, which is the average error caused by quantization of the real and imaginary parts of harmonic source current. The real and imaginary parts of actual instrument measurements on lines 4-5, 12-6 and 12-13 were each given $\sigma = 0.001$ pu, which is 1% of the full scale reading.

The root mean square (rms) of the errors for the neural network estimates and state estimates are shown at the top of Fig. 3.4. The rms of error is defined as the square root of the mean of the squared difference between the model harmonic complex current and the estimated complex current (from neural network or state estimation) at buses 4, 5, 6 and 14. The root mean square of the standard deviations for the neural network estimates (obtained from diagonal elements of R_h) and state estimates (obtained from diagonal elements of P_{i_h}) are also shown in Fig. 3.4. The error in the neural network estimate reflects quantization error from the 3-bit binary neural network output and the approximate nature of the learned input-output classifications. As Fig. 3.4 shows, the rms of errors (as well as rms of standard deviations) for the state estimates are always smaller than the rms of errors (as well as rms of standard deviations) for the neural network estimates, which indicates that the state estimator generally "pulls" all the pseudomeasurements toward the correct model values. The plots comparing the magnitudes in the lower part of Fig. 3.4 sometimes mask the improvement in the state estimates because phase angle errors are not shown. Estimates for the 7-th, 11-th and 13-th harmonics showed a similar pattern.

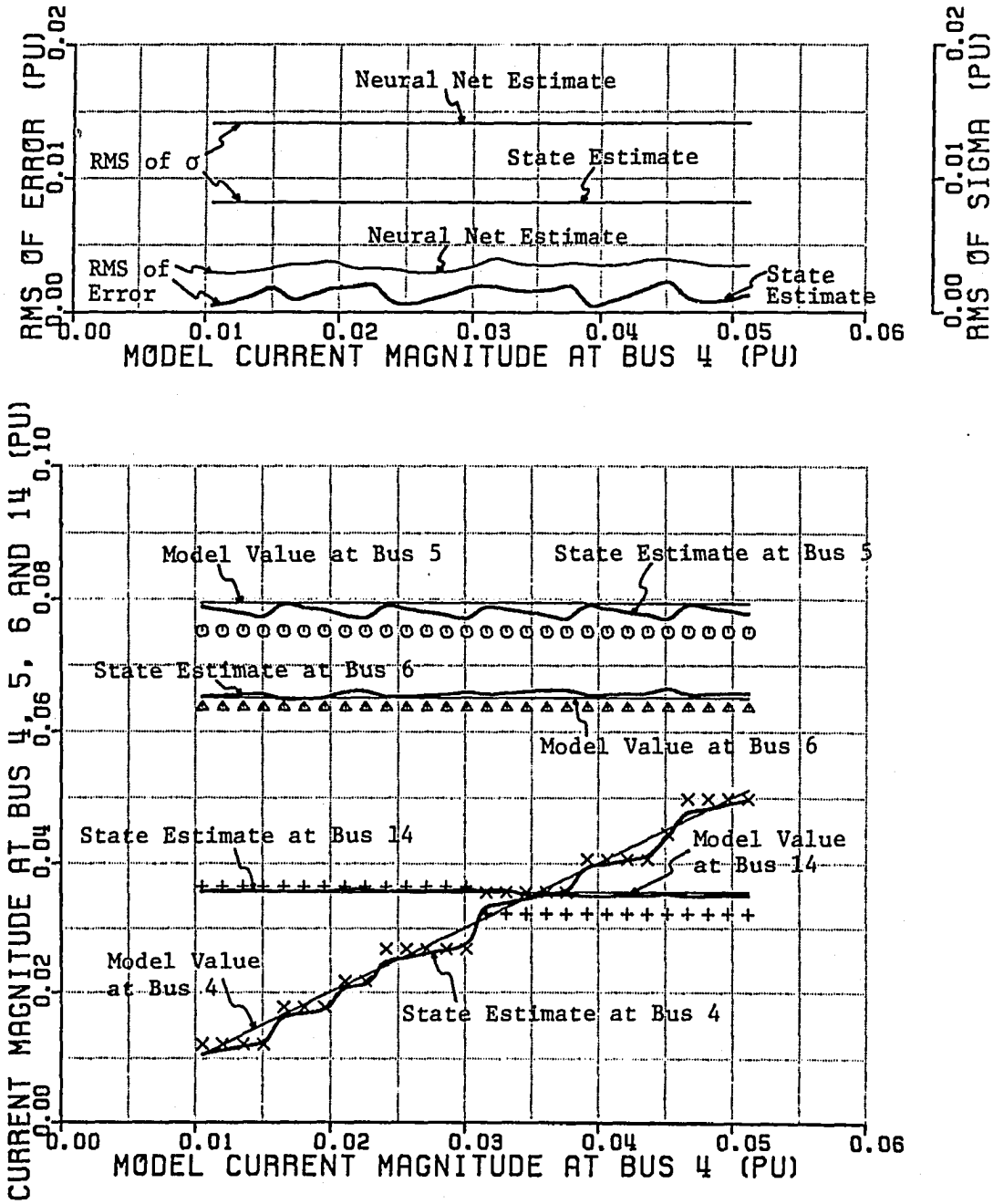

Fig. 3.4 Estimated 5-th Harmonic Current Magnitudes at Buses 4, 5, 6 and 14, and RMS of Errors and Sigmas versus Model Current Magnitude at Bus 4 for First Test

x x x Neural Network Estimate at Bus 4
o o o Neural Network Estimate at Bus 5
Δ Δ Δ Neural Network Estimate at Bus 6
+ + + Neural Network Estimate at Bus 14

To show the effect of using neural network estimates, state estimation was applied without the benefit of pseudomeasurements from the neural networks. As an underspecified state estimation problem (m < n), the measurement matrix A_h in eqn (3.11) is altered in accordance with Ref. [62], and the estimated harmonic current vector, i_h, in eqn (3.12) becomes

$$i_h = A'_h \left(A_h A'_h\right)^{-1} i_{hm} . \tag{3.17}$$

The state estimates for the harmonic current magnitudes injected at buses 4, 5, 6 and 14 from the first test are calculated by eqn (3.17) and the results are then plotted in the lower part of Fig. 3.5. It is noted that in this case the magnitude of i_h is minimized. The rms of error for these state estimates (as shown at the top of Fig.3.5) is larger than the rms of error with pseudomeasurements (as shown at the top of Fig.3.4).

For the second test of monitoring buses 4, 5, 6 and 14, the thyristor-controlled load at bus 4 was given an increasing firing angle with a constant and unknown resistive load while the rectifier loads at buses 5, 6 and 14 were still kept constant at unknown magnitudes. Fig. 3.6 is a plot of the magnitudes of fifth harmonic injected model currents, the current magnitudes estimated by the neural networks, and the current magnitudes estimated by the state estimator at buses 4, 5, 6 and 14 versus the load firing angle at bus 4. The state estimation is less effective in improving the neural network estimates at buses 4 and 5, which are closely linked and difficult to be distinguished from the harmonic current detector on line 4-5.

To further test the effectiveness of the method, the harmonic generated loads at buses 4, 5, 6 and 14 in the third test were randomly varied. The resulting estimates and the correct model values for the harmonic currents (both magnitudes and phase angles) injected at the four buses are tabulated in Table 3.2. The last two columns are the rms of errors (square root of the mean squared error magnitude for all four buses) for the neural network

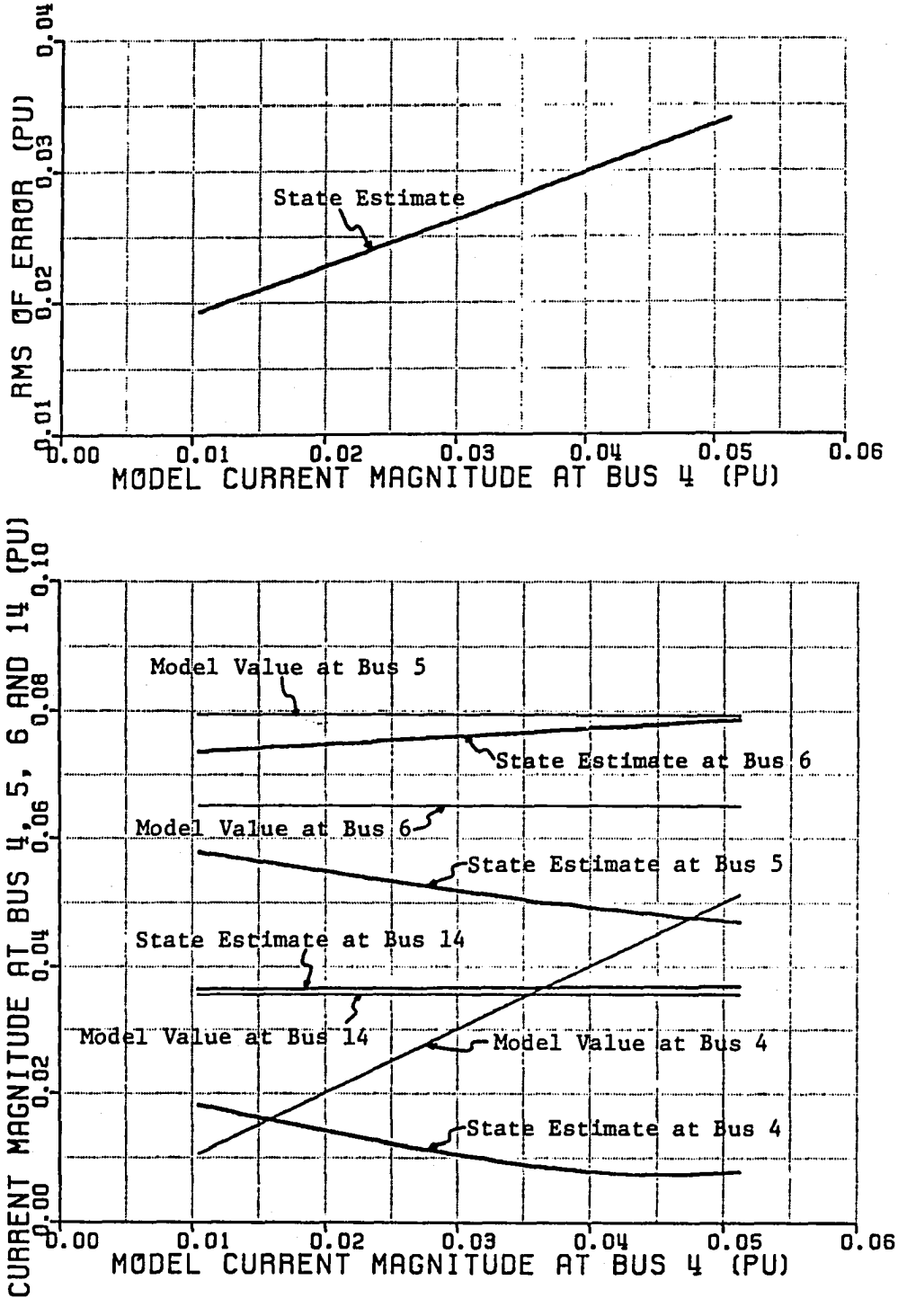

Fig. 3.5 Estimated 5-th Harmonic Current Magnitudes at Buses 4, 5, 6 and 14, and RMS of Error versus Model Current Magnitude at Bus 4 for First Test (without Neural Network estimates)

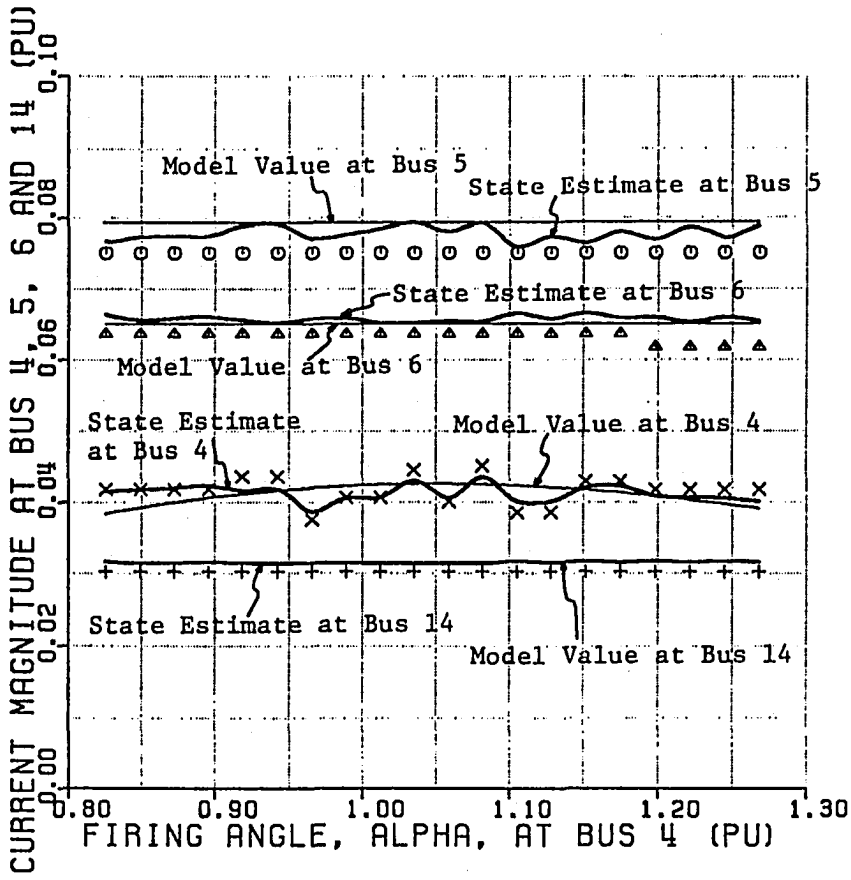

Fig. 3.6 Estimated 5-th Harmonic Current Magnitudes at Buses 4, 5, 6 and 14 versus Firing Angle (α) at Bus 4 for Second Test

x x x Neural Network Estimate at Bus 4
o o o Neural Network Estimate at Bus 5
Δ Δ Δ Neural Network Estimate at Bus 6
+ + + Neural Network Estimate at Bus 14

TABLE 3.2 HARMONIC SOURCE ESTIMATES FOR RANDOMLY VARYING LOADS

	I_{h4}			I_{h5}			I_{h6}			I_{h14}				
	Estimate Value		Correct	Estimate Value		Correct	Estimate Value		Correct	Estimate Value		Correct	RMS of Error [pu]	
	Neural Net	State Est.	Model Value	Neural Net	State Est.	Model Value	Neural Net	State Est.	Model Value	Neural Net	State Est.	Model Value	Neural Net	State Est.
1.	0.032 ∠65.0°	0.0344 ∠65.6°	0.0345 ∠65.0°	0.056 ∠93.6°	0.055 ∠93.9°	0.0546 ∠93.8°	0.069 ∠119.5°	0.071 ∠117.°	0.072 ∠116.7°	0.053 ∠114.6°	0.052 ∠114.2°	0.0518 ∠114.5°	0.00285	0.00055
2.	0.023 ∠28.2°	0.024 ∠26.4°	0.0241 ∠20.0°	0.045 ∠95.7°	0.044 ∠96.6°	0.0425 ∠96.0°	0.052 ∠119.°	0.048 ∠119.5°	0.049 ∠119.5°	0.06 ∠113.4°	0.064 ∠113.°	0.065 ∠112.9°	0.00333	0.00180
3.	0.0347 ∠-6.6°	0.0355 ∠-3.6°	0.0362 ∠-3.3°	0.085 ∠92.4°	0.091 ∠91.6°	0.0906 ∠91.4°	0.041 ∠121.5°	0.036 ∠119.4°	0.0355 ∠119.3°	0.06 ∠113.4°	0.059 ∠113.5°	0.059 ∠113.8°	0.00396	0.00044
4.	0.0323 ∠31.7°	0.029 ∠27.7°	0.03 ∠35.4°	0.075 ∠91.7°	0.079 ∠91.6°	0.082 ∠91.8°	0.059 ∠111.8°	0.059 ∠116.4°	0.057 ∠117.6°	0.042 ∠116.9°	0.045 ∠116.5°	0.0453 ∠115.7°	0.00545	0.00327
5.	0.012 ∠-114.°	0.009 ∠-92.°	0.013 ∠-75.6°	0.045 ∠95.7°	0.036 ∠100.°	0.032 ∠98.2°	0.041 ∠121.5°	0.027 ∠124.°	0.029 ∠123.°	0.031 ∠115.7°	0.021 ∠119.3°	0.02 ∠120.9°	0.01134	0.00378
6.	0.042 ∠-96.8°	0.052 ∠-98.6°	0.05 ∠-92.7°	0.085 ∠93.0°	0.102 ∠90.7°	0.105 ∠87.7°	0.087 ∠113.°	0.0967 ∠111.°	0.097 ∠112.8°	0.031 ∠115.7°	0.029 ∠116.6°	0.028 ∠117.6°	0.01293	0.00464
7.	0.017 ∠39.2°	0.0133 ∠1.88°.	0.014 ∠-43.5°	0.065 ∠94.0°	0.073 ∠91.9°	0.0682 ∠94.3°	0.041 ∠121.5°	0.032 ∠124.6°	0.033 ∠120.4°	0.06 ∠113.4°	0.066 ∠112.9°	0.069 ∠112.3°	0.01227	0.00650
8.	0.042 ∠-96.8°	0.05 ∠-99.0°	0.048 ∠-83.2°	0.095 ∠92.7°	0.122 ∠90.0°	0.125 ∠84.4°	0.087 ∠113.°	0.12 ∠105.6°	0.121 ∠108.4°	0.06 ∠113.4°	0.079 ∠107.9°	0.08 ∠108.1°	0.02731	0.01000

and state estimates. The results show substantial estimation errors only when data fall significantly outside the training range, as they do in rows 7 and 8. The seventh row of Table 3.2 shows a poor neural network estimate of phase angle and magnitude of the harmonic source at bus 4, which caused an increased state estimation error at bus 5. The last row of the Table shows significant neural network magnitude errors at buses 5, 6 and 14. A trade-off among the errors at the four buses by the state estimator resulted an increasing state estimation error at bus 4.

For the fourth simulation, to test the estimator's effectiveness in identifying unknown harmonic sources, bus 10 was considered a "suspected" bus by including it as a current injection source with a pseudomeasurement of zero in the state estimator equation. As an uncertain bus, its standard deviation was set to $\sigma = 0.05$ pu in the noise covariance matrix corresponding to the average magnitude of the harmonic sources. Fig. 3.7 is a plot of the magnitudes of fifth harmonic injected model currents, the current magnitudes estimated by the neural networks, and the current magnitudes estimated by the state estimator at buses 4, 5, 6, 10 and 14 versus the fifth harmonic model current magnitudes which were injected at bus 10. The rms of error shown at the top of Fig.3.7 includes the error of the assumption that the neural network estimate for harmonic injection at bus 10 is zero. Thus, the state estimator monitors the suspected bus 10 injections by using the pseudomeasurements from the neural networks, which have a lower σ, or less uncertainty, than the bus 10 pseudomeasurement of zero. This suggests that the method can be extended to identify and monitor harmonic sources for which the neural network has not been specifically trained.

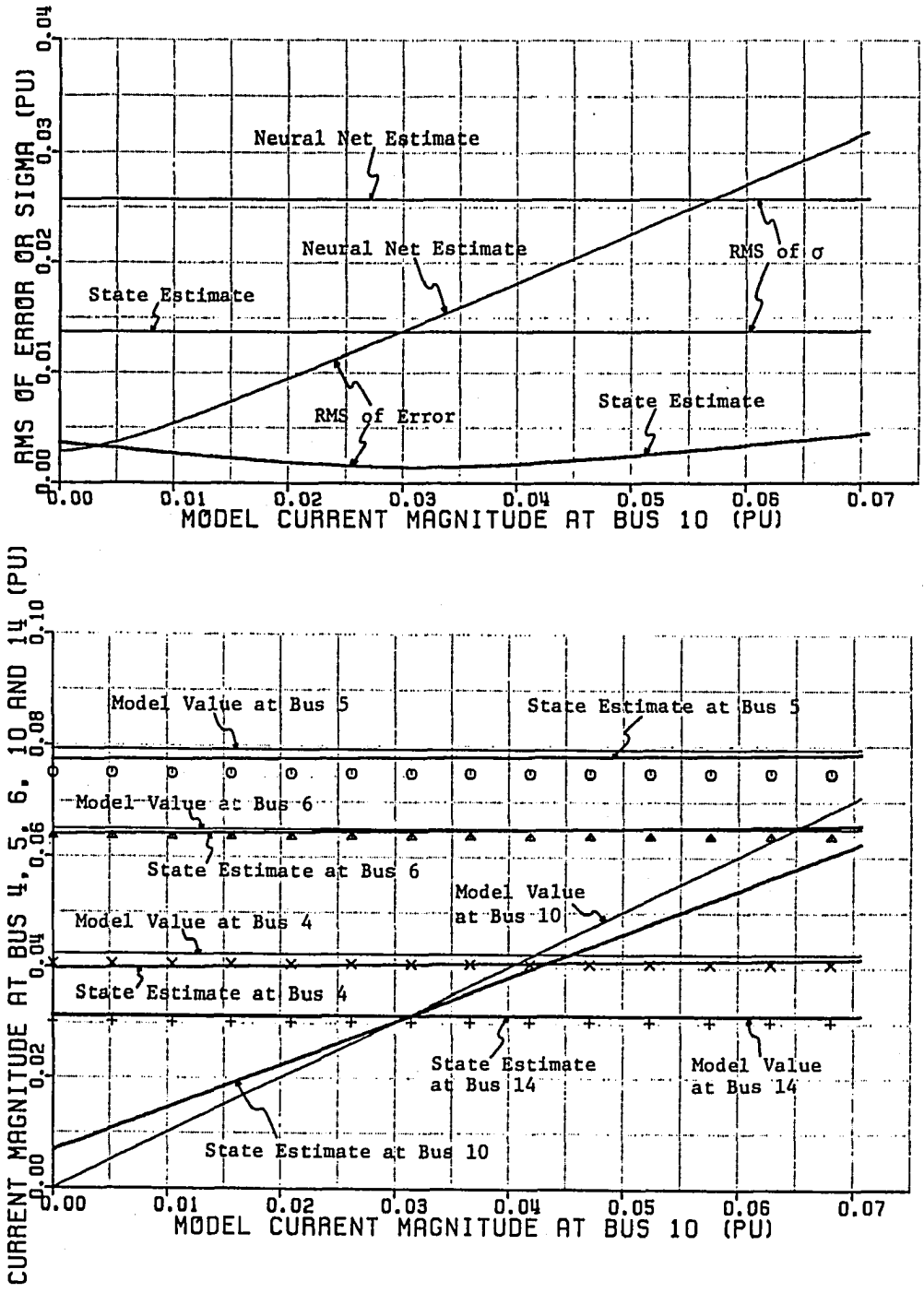

Fig. 3.7 Estimated 5-th Harmonic Current Magnitudes at Buses 4, 5, 6, 10 and 14, and RMS of Errors and Sigmas versus Model Current Magnitude at Bus 10 for Fourth Test

x x x Neural Network Estimate at Bus 4
o o o Neural Network Estimate at Bus 5
Δ Δ Δ Neural Network Estimate at Bus 6
+ + + Neural Network Estimate at Bus 14

CHAPTER 4

OPTIMUM FILTER DESIGN WITH MULTIPLE HARMONIC SOURCES

If the energy supplier (utility) wishes to reduce voltage harmonic distortion, he may locate the harmonic source and place a filter there. However, if the harmonic current sources are numerous, as they often are, filtering each harmonic source becomes impractical and uneconomical, and filtering the largest harmonic source may not be optimal for all utility customers. In such situations, it may be desirable for an energy supplier to minimize voltage harmonic distortion for the entire feeder. Techniques for such feeder filtering with multiple harmonic sources have been discussed in Refs [28-30], but the solution approach is qualitative and intuitive. Quantitative minimization of harmonic distortion for all feeder buses by optimizing filter admittances at harmonic frequencies has not been done.

In finding the optimum filters for a feeder, the problem of shifting system response caused by variable compensating capacitors must be taken into account . In Refs [28-30], it is suggested that the filters be selected with switched capacitor banks at their "worst case" values. The worst case is found by an exhaustive search of all switched capacitor combinations for all possible resonant conditions. After placing the filter, the search is done again to assure that there is no new resonance. This approach requires iteration and may not converge.

Another question that arises in distribution feeder filtering, in addition to filter admittance optimization, is filter placement. Best results are obtained with properly placed filters. Filter components for all harmonic frequencies need not be at the same bus. Filter placement is discussed in Refs [28-30] which suggest the simple rule of placing the filter at the capacitor bank farthest from the substation. However, this rule is not always best for the case of distributed harmonic sources.

In this chapter, the three issues relating to minimizing harmonic voltage distortion

for the entire feeder buses with multiple and balanced or unbalanced harmonic sources are addressed [45]. First, a measure of combined bus distortion for the entire feeder is introduced and a method of finding optimum filter admittances with varying compensating capacitors is presented. Symmetrical components are used for the unbalanced harmonic source case. Then, the problem of filter placement is explored. Finally, filter realization with the lowest cost (size), including sensitivity analysis, is discussed. An example 35-bus distribution feeder is simulated and the results are compared to the conventional filter design procedures.

4.1 Feeder Voltage Harmonic Reduction

The distribution feeder under study is considered to serve a large number of nonlinear loads. Therefore, harmonic current sources and compensating capacitors are numerous and widely distributed throughout the feeder. The distribution feeder parameters, harmonic sources and capacitors (fixed or variable) are assumed to be known a priori. If harmonic sources are not known, they can be monitored and identified by the method discussed in Chapter 3.

The objective is to select and place filters to minimize the combined total harmonic distortion (*CTHD*) of all buses on an n-bus distribution feeder. *CTHD* is defined as a weighted root mean square of the individual bus *THD*s:

$$CTHD = \sqrt{\frac{1}{n} \sum_{i=1}^{n} W_i \, THD_i^2} \tag{4.1}$$

where THD_i is the total harmonic distortion at bus i averaged for all three phases, and W_i is the weight. Weighting factors are used to emphasize significant *THD*s at critical buses.

CTHD will be minimized under a condition of known distributed harmonic current sources, taking into account several variable compensating capacitors. To create a "worst case", these capacitors will be considered to be variable from zero to their maximum

values. The possibility of unbalanced harmonic current sources will also be considered. Using this minimization, the problem of filter placement will be explored and some conclusions reached.

4.2 Objective Function

For a balanced and symmetrical n-bus distribution system, the harmonic voltages along the feeder for harmonic order h can be calculated as in eqns (2.14) - (2.15),

$$\left[V_{bus}^{h}\right] = \left[Z_{bus}^{h}\right]\left[I_{bus}^{h}\right] \tag{4.2}$$

where $\left[V_{bus}^{h}\right] = \left[V_1^h\, V_2^h \cdots V_n^h\right]^T$ = (n × 1) bus harmonic voltage vector,

$\left[I_{bus}^{h}\right] = \left[I_1^h\, I_2^h \cdots I_n^h\right]^T$ = (n × 1) bus harmonic current injection vector,

$$\left[Z_{bus}^{h}\right] = \begin{bmatrix} Z_{11}^h & Z_{12}^h & \cdots & Z_{1n}^h \\ Z_{21}^h & Z_{22}^h & \cdots & Z_{2n}^h \\ \vdots & \vdots & \cdots & \vdots \\ Z_{n1}^h & Z_{n2}^h & \cdots & Z_{nn}^h \end{bmatrix} = (n \times n) \text{ bus impedance matrix,} \tag{4.3}$$

and superscript T indicates transposition.

Total harmonic distortion (*THD*) for voltage at bus i is defined as in eqn (2.13),

$$THD_i = \frac{1}{\left|V_i^1\right|}\sqrt{\sum_{h>1}\left|V_i^h\right|^2} \tag{4.4}$$

where V_i^1 and V_i^h are the fundamental and h-th harmonic voltages at bus i.

Assuming fundamental frequency voltages at all buses constant and equal to 1.0 pu, the combined total harmonic distortion, *CTHD*, is obtained by substituting (4.4) into (4.1),

$$CTHD = \sqrt{\frac{1}{n}\sum_{h>1}\left[V_{bus}^{h}\right]^{*T}[W]\left[V_{bus}^{h}\right]} \qquad (4.5)$$

where superscript * indicates conjugation of complex variables, and [W] is the diagonal matrix of weights, W_i.

In a distribution system with compensating capacitors, if there are j variable capacitors with admittances varying from 0 to $Y_{cl\,\max}$ $(l = 1,2,\ldots,j)$, eqn (4.5) is averaged over all variable capacitor value ranges,

$$CTHD = \sqrt{\frac{1}{n\,m_1 \ldots m_j}\sum_{h>1}\sum_{k_1=0}^{m_1}\cdots\sum_{k_j=0}^{m_j}\frac{\left[V_{bus}^{h}(k_1\Delta Y_{c1},..,k_j\Delta Y_{cj})\right]^{*T}[W]}{\left[V_{bus}^{h}(k_1\Delta Y_{c1},..,k_j\Delta Y_{cj})\right]}} \qquad (4.6)$$

where $\Delta Y_{cl} = Y_{cl\,\max}/m_l$, is the capacitor admittance increment and m_l is the number of equal switching steps.

For the case of unbalanced harmonic current sources, the equations shown above are still valid, except the scalar notations of voltage, current and impedance for each bus on the right hand side of eqn (4.3) are replaced by their corresponding vector notations for representing the positive-, negative- and zero-sequence components (using the Fortescue transformation). The bus harmonic voltage and current vectors for harmonic order h are now (3n × 1) vectors:

$$\left[V_{s,bus}^{h}\right] = \left[\left[V_{s,1}^{h}\right]\cdots\left[V_{s,i}^{h}\right]\cdots\left[V_{s,n}^{h}\right]\right]^{T},$$

$$\left[I_{s,bus}^{h}\right] = \left[\left[I_{s,1}^{h}\right]\cdots\left[I_{s,i}^{h}\right]\cdots\left[I_{s,n}^{h}\right]\right]^{T}, \qquad (4.7)$$

where subscript s denotes sequence components,

$$\left[V_{s,i}^{h}\right] = \left[V_{+i}^{h}\ V_{-i}^{h}\ V_{oi}^{h}\right],\quad \left[I_{s,i}^{h}\right] = \left[I_{+i}^{h}\ I_{-i}^{h}\ I_{oi}^{h}\right],$$

and +, -, o represent positive-, negative- and zero-sequence components, respectively. The

bus impedance matrix is a (3n x 3n) matrix:

$$[Z^h_{s,bus}] = \begin{bmatrix} [Z^h_{s,11}] & [Z^h_{s,12}] & \cdots & [Z^h_{s,1n}] \\ [Z^h_{s,21}] & [Z^h_{s,22}] & \cdots & [Z^h_{s,2n}] \\ \vdots & \vdots & \cdots & \vdots \\ [Z^h_{s,n1}] & [Z^h_{s,n2}] & \cdots & [Z^h_{s,nn}] \end{bmatrix} \tag{4.8}$$

where $[Z^h_{s,nn}] = diag\,[Z^h_{+nn}\ \ Z^h_{-nn}\ \ Z^h_{onn}]$.

Then, replacing $[V^h_{bus}]$ in eqn (4.6) by $[V^h_{s,bus}]$ in eqn (4.7), the objective function of eqn (4.6) is now expressed in terms of symmetrical components.

4.3 Harmonic Distribution System Model

Harmonic-producing (nonlinear) loads can be modeled as ideal harmonic current sources or as harmonic current sources in parallel with load impedances. The ideal harmonic current source model is adequate for a wide range of circuit conditions when the voltage distortion is not greater than 10%. When the distortion is high (over 10%), the harmonic current source model in parallel with load impedance is necessary.

Linear loads such as induction motors are represented as an equivalent R-L in series. For loads which are not well defined, a parallel R-L representation is used. Transformers are represented as an equivalent leakage inductance or an equivalent leakage resistance and inductance in series. For analysis of low frequency harmonics (up to 17-th harmonic), relatively short overhead distribution lines are represented as nominal pi-equivalent circuits connected in cascade. The other shunt capacitances that are included in the analysis are the compensating capacitors. For higher harmonic frequencies, the lines are represented as the exact pi-equivalent circuits. All of these system component models have been discussed in Chapter 2, and their equivalent circuits are shown in Table 2.1.

4.4 Optimum Filter Admittance

To minimize *CTHD* with respect to filter admittances, the Steepest Descent method is used. Filter admittances at relevant harmonic frequencies are independent variables. The actual filter components are then realized from optimum filter admittances. Minimization of *CTHD* is obtained by minimizing eqn (4.6) separately for each harmonic frequency. The superscript h is omitted hereafter for clarity.

4.4.1 One Filter

When a filter with admittance Y_p, is placed at bus p, the bus voltages are:

$$V_i = V_i^0 - \frac{Z_{ip} Y_p V_p^0}{Z_{pp} Y_p + 1}; \qquad i = 1, 2, \ldots\ldots, n, \quad i \neq p,$$

$$V_p = \frac{V_p^0}{Z_{pp} Y_p + 1}; \tag{4.9}$$

where V_i^0, V_p^0 are the voltages at buses i and p before placing the filter, and V_i, V_p are the voltages at bus i and p after placing the filter. V_i^0, V_p^0 are computed from eqn (4.2), where the original bus impedance matrix is constructed without filter. By substituting eqn (4.9) into eqn (4.6) for each harmonic frequency, the objective function, *CTHD*, can now be minimized with respect to Y_p.

For the unbalanced harmonic source case, when a 3-phase filter with admittance $Y_{p\varphi}$ (φ = *phase a, b, c*) is placed at bus p, the bus voltages are:

$$\left[V_{s,i}\right] = \left[V_{s,i}^0\right] - \left[Z_{s,ip}\right]\left[Y_{s,p}^f\right]\left[V_{s,p}\right], \quad i = 1, 2, \ldots, n, \quad i \neq p,$$

$$\left[V_{s,p}\right] = [YP]^{-1}\left[V_{s,p}^0\right], \tag{4.10}$$

where $[YP] = [I] + \left[Z_{s,pp}\right]\left[Y_{s,p}^f\right]$,

$$\left[Y^{f}_{s,p}\right]=\begin{bmatrix} Y_o & Y_- & Y_+ \\ Y_+ & Y_o & Y_- \\ Y_- & Y_+ & Y_o \end{bmatrix},$$

$$\begin{aligned} Y_+ &= \left(Y_{pa} + \alpha Y_{pb} + \alpha^2 Y_{pc}\right)/3, \\ Y_- &= \left(Y_{pa} + \alpha^2 Y_{pb} + \alpha Y_{pc}\right)/3, \\ Y_o &= \left(Y_{pa} + Y_{pb} + Y_{pc}\right)/3, \end{aligned} \tag{4.11}$$

$\alpha = 1\angle 120°$ and $[I]$ is a (3 × 3) identity matrix. $\left[V^{0}_{s,i}\right]$ and $\left[V^{0}_{s,p}\right]$ are the sequence voltages at buses i and p before placing the filter. Note that Y_+ and Y_- in eqn (4.11) are derived for positive-sequence harmonic currents (h = 7 and 13). They are interchanged for negative-sequence harmonic currents (h = 5 and 11). By substituting eqn (4.10) into eqn (4.7) and then replacing $[V_{bus}]$ in eqn (4.6) by $[V_{s,bus}]$ in eqn (4.7), the objective function, *CTHD*, becomes a function of three variables (Y_{pa}, Y_{pb} and Y_{pc}). For the balanced harmonic source case, the 3-phase filter admittances (Y_{pa}, Y_{pb} and Y_{pc}) are identical, but for the unbalanced case, they are not identical.

4.4.2 Two Filters

Many distribution systems have more than one major feeder branch. In this case, a single filtering scheme might not be sufficient to reduce the harmonic distortion at all buses on the feeder, because the filter will tend to be most effective at the buses on the feeder branch where it is located and leave the distortion at other buses quite high. Therefore, two or more filters may be required, one at each major feeder branch [28,29].

For the case of a distribution system with two major branches, the bus voltage equations for two filters are derived below. For a distribution system with three or more major branches, equations can be extended to three or more filters. For two filters, one with admittance Y_p placed at bus p and the other with admittance Y_q placed at bus q, the bus voltages along the feeder buses are:

$$V_i = V_i^0 - \frac{\{Y_p Z_{ip}(Y_q Z_{qq}+1) - Y_p Y_q Z_{iq} Z_{pq}\}V_p^0 + \{Y_q Z_{iq}(Y_p Z_{pp}+1) - Y_p Y_q Z_{ip} Z_{pq}\}V_q^0}{(Y_p Z_{pp}+1)(Y_q Z_{qq}+1) - Y_p Y_q Z_{pq}^2};$$

$$i = 1, 2, \ldots\ldots, n \ , \ i \neq p \ , \ i \neq q \ ,$$

$$V_p = \frac{(Y_q Z_{qq}+1)V_p^0 - Y_q Z_{pq} V_q^0}{(Y_p Z_{pp}+1)(Y_q Z_{qq}+1) - Y_p Y_q Z_{pq}^2};$$

$$V_q = \frac{(Y_p Z_{pp}+1)V_q^0 - Y_p Z_{pq} V_p^0}{(Y_p Z_{pp}+1)(Y_q Z_{qq}+1) - Y_p Y_q Z_{pq}^2}. \qquad (4.12)$$

By substituting eqn (4.12) into eqn (4.6), the objective function becomes a function of two variables (Y_p and Y_q), which can be minimized with respect to these two variables.

For the unbalanced harmonic source case with two 3-phase filters, one with admittance $Y_{p\varphi}$ ($\varphi = a, b, c$) placed at bus p and the other with admittance $Y_{q\varphi}$ ($\varphi = a, b, c$) placed at bus q, the bus voltages are:

$$[V_{s,i}] = [V_{s,i}^0] - [Z_{s,ip}][Y_{s,p}^f][V_{s,p}] - [Z_{s,iq}][Y_{s,q}^f][V_{s,q}], \quad i = 1, 2, \ldots, n, \ i \neq p, \ i \neq q,$$

$$[V_{s,p}] = \left[[YP] - [Z_{s,pq}][Y_{s,q}^f][YQ]^{-1}[Z_{s,pq}][Y_{s,p}^f] \right]^{-1} [A],$$

$$[V_{s,q}] = \left[[YQ] - [Z_{s,pq}][Y_{s,p}^f][YP]^{-1}[Z_{s,pq}][Y_{s,q}^f] \right]^{-1} [B], \qquad (4.13)$$

where $[A] = [V_{s,p}^0] - [Z_{s,pq}][Y_{s,q}^f][YQ]^{-1}[V_{s,q}^0]$,

$[B] = [V_{s,q}^0] - [Z_{s,pq}][Y_{s,p}^f][YP]^{-1}[V_{s,p}^0]$,

$$[YQ] = [I] + \left[Z_{s,qq}\right]\left[Y^{f}_{s,q}\right],$$

and $\left[Y^{f}_{s,q}\right]$ is the same as in eqn (4.11) with subscript p changed to subscript q. By substituting eqn (4.13) into eqn (4.7) and then replacing $[V_{bus}]$ in eqn (4.6) by $\left[V_{s,bus}\right]$ in eqn (4.7), the objective function is now a function of six variables (Y_{pa}, Y_{pb}, Y_{pc}, Y_{qa}, Y_{qb}, and Y_{qc}).

4.4.3 Minimization Technique

The Steepest Descent algorithm used for minimization is outlined in Appendix A. The combined total harmonic distortion is minimized with respect to six variables (two 3-phase filter admittances) at each harmonic frequency.

4.5 Optimum Filter Location

If a feeder is to have only one optimum filter for each harmonic, the best location can be found by simulating *CTHD* with an optimum filter placed at each bus until the location with minimum *CTHD* is found. However, this approach is time consuming if there are many buses on the feeder, or if it is necessary to locate two filters on the feeder.

In the case of a single feeder branch with many buses injecting harmonic currents, a directed search, such as the Golden Section method, may be useful because minimum values of *CTHD* tend to form a unimodal function of filter distance from the end of the feeder. Such a search must be done over the length of each branch of the feeder. The Golden Section strategy used for the simulation study is given below. The notation is :

p_u, p_l - the upper and lower bound of the interval, measured in length,

b_u, b_l - the nearest buses to p_u and p_l, respectively,

p_1, p_2 - the points within the interval, measured in length,

b_1, b_2 - the nearest buses to p_1 and p_2, respectively,

$g(b_i)$ - the measured value of bus i in length, and

$f(b_i)$ - the minimum value of *CTHD* when a filter is placed at bus i.

Given the length of a feeder branch equal to d, $p_l = 0$, $p_u = d$, the following steps illustrate the algorithm:

1. Calculate $p_1 = p_l + 0.38\,(p_u - p_l)$, find b_1,
   $p_2 = p_u - 0.38\,(p_u - p_l)$, find b_2,
   evaluate $f(b_1)$, $f(b_2)$.
2. If $f(b_1) \leq f(b_2)$, go to 6.
3. Otherwise, set $b_l = b_1$, $p_l = g(b_1)$ and $f(b_l) = f(b_1)$.
4. Set $b_1 = b_2$, $p_1 = g(b_2)$ and $f(b_1) = f(b_2)$.
5. Calculate $p_2 = p_u - 0.38\,(p_u - p_l)$ and find b_2, evaluate $f(b_2)$ and go to 9.
6. Set $b_u = b_2$, $p_u = g(b_2)$ and $f(b_u) = f(b_2)$.
7. Set $b_2 = b_1$, $p_2 = g(b_1)$ and $f(b_2) = f(b_1)$.
8. Calculate $p_1 = p_l + 0.38\,(p_u - p_l)$ and find b_1, evaluate $f(b_1)$.
9. If (b_l, b_u) or (b_l, b_1, b_2, b_u) are adjacent buses, then find the minimum of $f(b_i^*)$; b_i^* is the optimum filter location and stop. Otherwise, go to 2.

For the two filter case in an n-bus distribution system with feeder branches, the suggestion of [28,29], placing one filter per feeder branch, is followed. One filter is placed in the m-bus feeder branch at the bus with highest distortion level, and the other filter is then placed at the bus in the branch with (n-m) buses. In total, there are m(n-m) combination of locations to be searched for the best two locations. The Golden Section search can be applied to the filter being placed among the (n-m) buses, each to achieve minimum *CTHD*. This result is then used in the directed search in the m-bus branch.

4.6 Filter Realization

A one-port filter with multiple branches of L and/or C circuits can be constructed at the optimum bus location using filter admittances obtained from minimization of eqn (4.6). The values of L's and C's in the filter are selected such that the total filter cost is minimized. For M harmonics (with harmonic order, h > 1), the one-port filter consists of

M branches, each composed of L-C in series, as shown in Fig. 4.1.

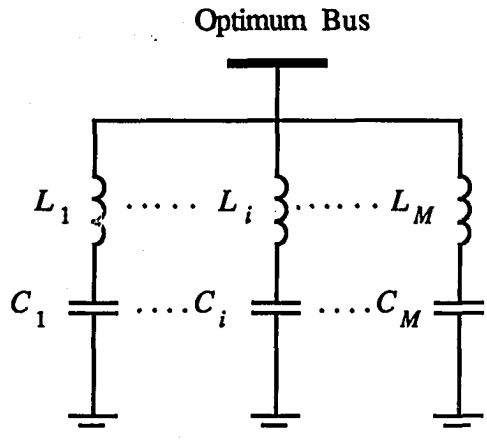

Fig. 4.1 A One-Port Filter Configuration

The admittance at harmonic order h is

$$Y_f(h) = \frac{S_1\, h}{P_1^2 - h^2} + \cdots + \frac{S_i\, h}{P_i^2 - h^2} + \cdots + \frac{S_M\, h}{P_M^2 - h^2} \qquad (4.14)$$

where $S_1 = \frac{1}{\omega L_1}, \ldots, S_i = \frac{1}{\omega L_i}, \ldots, S_M = \frac{1}{\omega L_M},$

$$P_1^2 = \frac{1}{\omega^2 L_1 C_1}, \ldots, P_i^2 = \frac{1}{\omega^2 L_i C_i}, \ldots, P_M^2 = \frac{1}{\omega^2 L_M C_M},$$

P_i is the order of pole (or tuned frequency) for filter branch i.

The total filter cost is

$$COST = U_L \sum_{i=1}^{M} VAR_{L_i} + U_C \sum_{i=1}^{M} VAR_{C_i}, \qquad (4.15)$$

where U_L and U_C are respectively the unit cost of reactor and capacitor per kVAR, and VAR_{L_i}, VAR_{C_i} are the voltampere ratings for reactor L_i and capacitor C_i.

The voltampere ratings required can be found from [47] :

$$VAR_{L_i} = \sqrt{\sum_h \left(|V^h| \frac{S_i h}{P_i^2 - h^2} \right)^2} \quad \sum_h \left(|V^h| \frac{h^2}{|P_i^2 - h^2|} \right) \quad kVAR$$

and

$$VAR_{C_i} = \sqrt{\sum_h \left(|V^h| \frac{S_i h}{P_i^2 - h^2} \right)^2} \quad \sum_h \left(|V^h| \frac{P_i^2}{|P_i^2 - h^2|} \right) \quad kVAR. \qquad (4.16)$$

The optimum filter realization is achieved by selecting P_i's such that the optimum filter admittances at harmonic frequencies of interest are satisfied by eqn (4.14), and the total filter cost defined by eqn (4.15) is minimized. The filter admittance defined by eqn (4.14) is always positive (capacitive) at fundamental frequency, which is desirable for reactive power compensation. However, a desired fundamental frequency admittance may be included in eqn (4.14) as a constraint.

4.7 Simulation Studies

A 35-bus radial distribution system taken from Ref. [29] was simulated in this study. The system consists of two 13.8 kV feeders fed from 230 kV source through a 24 MVA transformer. The transformer is Δ - Y connected, with neutral solidly grounded. One-line diagram of the distribution system is shown in Fig. 4.2.

The distribution lines are all overhead lines, except some short cables leading from the substation. There are nine capacitors totaling 10.6 MVAR for power factor correction. At first, only one variable capacitor is installed in the system and located at bus 29 with admittance varying from 0 to 0.05 pu (assuming 10 switching steps). The line and load impedances together with capacitor reactances and other system impedances for fundamental frequency are given in Appendix B. Loads are pessimistically assumed to include typical six-pulse rectifiers, which produce harmonics of order 5, 7, 11 and 13. The

other higher harmonics are considered small and ignored in this study. The magnitudes of harmonic currents generated by this type of load are 0.175 pu, 0.11 pu, 0.045 pu and 0.029 pu of the fundamental current for the 5-th, 7-th, 11-th and 13-th harmonics, respectively [47].

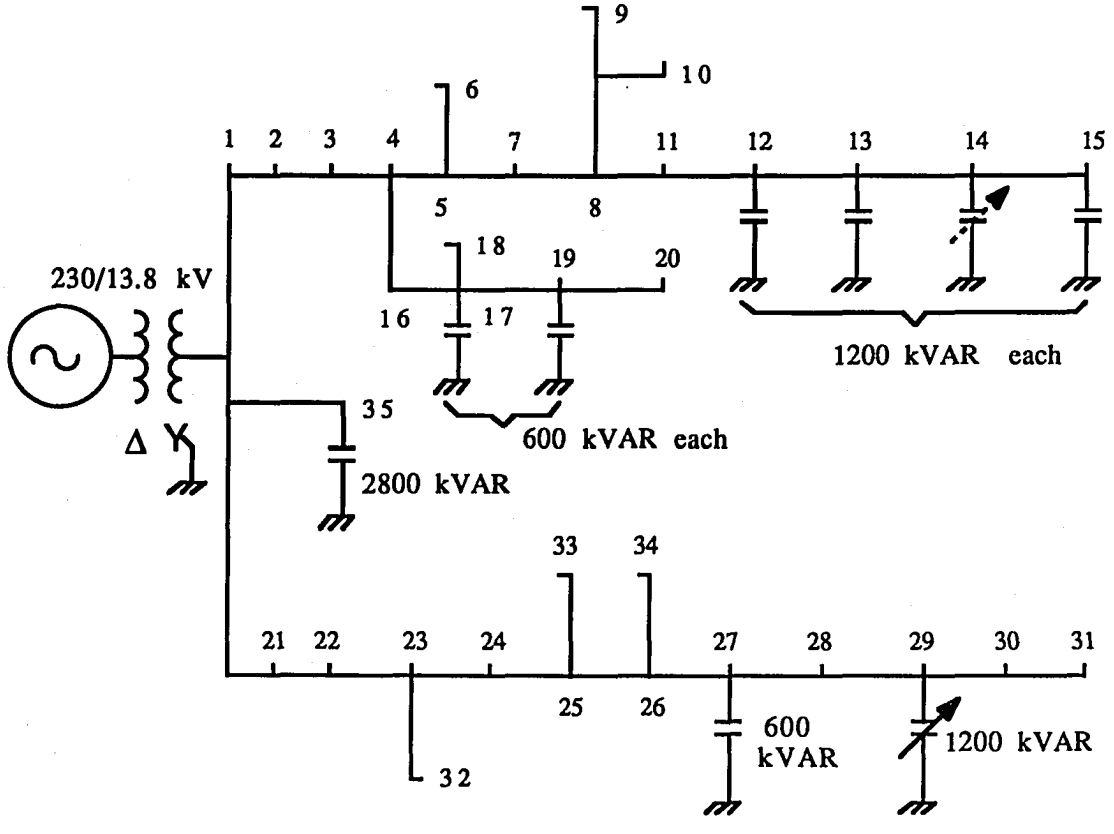

Fig. 4.2 One-Line Diagram of a 35-Bus Radial Distribution System

The nonlinear loads simulated in this study are assumed to total 0.25 pu current and therefore currents injected from all loads for each harmonic order h, I^h_{total}, are 25% of the above magnitudes. By assuming uniformly distributed harmonic currents at all buses, the magnitude of harmonic current injected at each bus is equal to 1/35 times I^h_{total}. The phase angles of all harmonic currents are taken to be 0.0° which is a pessimistic assumption. In

the system to be studied, it is assumed that harmonic distortion at every bus is equally important, therefore the weighting matrix [*W*] can be omitted from the equation.

4.7.1 One Filter

The results of four simulations with balanced harmonic current sources are given in Table 4.1. The first column of the Table shows the combined total harmonic distortion (*CTHD*) of the feeder before placing any filter, which is 4.562%. The total harmonic distortion (*THD*) at each bus is higher for the buses near the feeder end, where there are compensating capacitors. The plot of *THD* at each bus versus varying capacitive admittance at bus 29 before placing the filter is shown in Fig. 4.3. In the figure, the highest *THD* occurred at bus 31, with the *THD* (averaged over the range of variable capacitance) equal to 8.048%.

Table 4.1 Simulations with One Filter for Balanced Harmonic Current Sources

	No Filter	Tuned Filter at Bus 8	Tuned Filter at Bus 27	Optimum Filter at Bus 22
CTHD [%]	4.562	4.633	2.128	1.481
Most Distorted Bus	31	31	15	15
THD [%]	8.048	9.195	4.292	2.775

The second simulation shows a filter placed at bus 8, designed to reduce the harmonic distortion at only that bus. The filter is tuned exactly to the harmonic frequency. As shown in the second column of Table 4.1, the *CTHD* with such a filter and placement is higher than the one with no filter, because the distortion at other buses, such as bus 31, becomes higher (9.195%). However, when the tuned filter is placed at the most distorted bus (bus 27), which is also the placement suggested in [28,29], the *CTHD* is reduced by

more than one half, as shown in the third column. The most distorted bus is now bus 15 with a *THD* of 4.292%. The last column shows the result when the optimum filter is found by minimizing *CTHD* in eqn (4.6). The optimum location is bus 22. The *THD* at each bus is reduced to less than 2.775%.

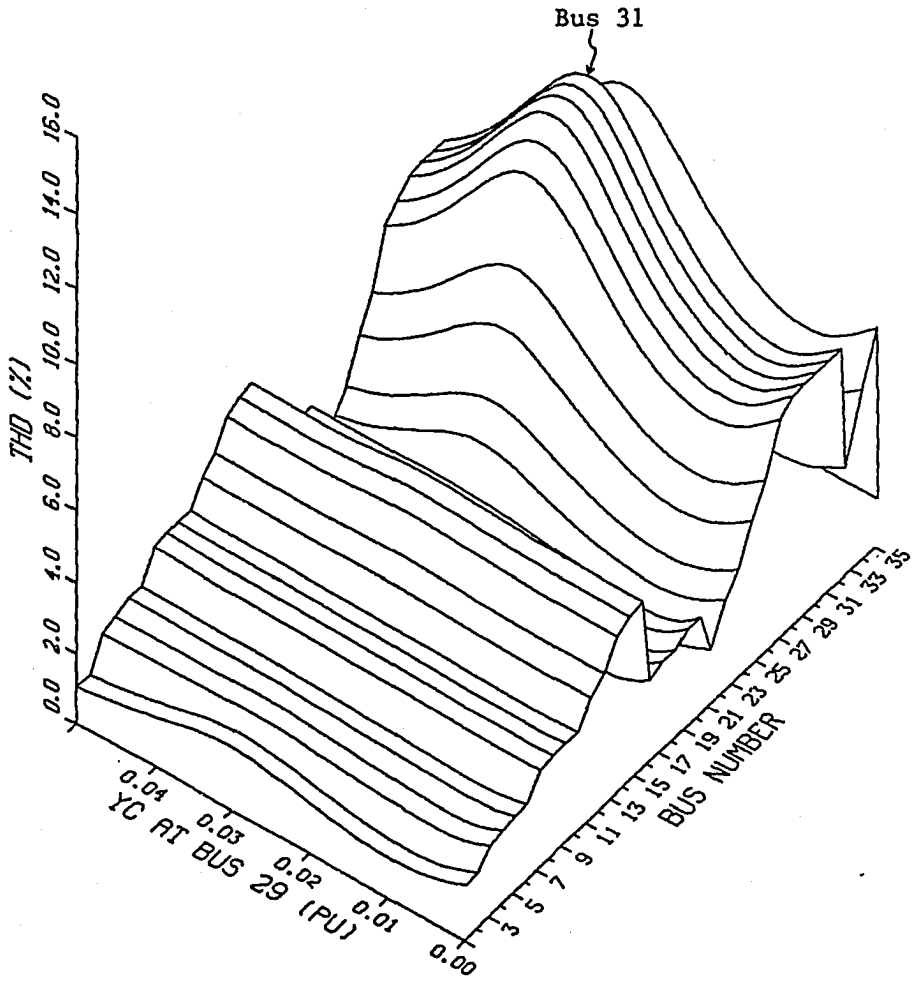

Fig. 4.3 3-D Plots of *THD*s versus Y_C at Bus 29 and Bus Number (Before Placing Filter)

The optimum filter admittances with two alternative corresponding filter realizations are given in Table 4.2. Note that the admittances are finite and positive indicating an optimum filter tuned above the harmonic frequency. This contrasts with the usual practice of tuning filters slightly below harmonic frequency to avoid attracting harmonic currents from other buses. In this case, it is desirable to attract some harmonic currents as the feeder inductance acts as part of the filter for the distributed harmonic sources.

Table 4.2 Optimum Filter Admittances and Realization at Bus 22

	Harmonic Order				
	5	7	11	13	
Admittance [pu]	2.527	2.298	1.491	1.200	
	Branch				
	L-C	L-C	L-C	L-C	L
1. Total Filter Rating = 5,601.0 kVAR (3-Phase)					
L [mH]	29.469	17.904	26.729	6.696	287.5
C [μF]	8.967	7.476	2.061	5.423	
Pole Order	5.160	7.250	11.300	13.920	
2. Total Filter Rating = 4,325.0 kVAR (3-Phase)					
L [mH]	66.365	59.770	58.466	49.249	
C [μF]	4.133	2.352	0.973	0.826	
Pole Order	5.065	7.075	11.120	13.155	

The first alternative for filter realization is selected when the fundamental frequency filter admittance has to be zero. The filter consists of five branches: four branches of L-C and one branch of L. If capacitive admittance at fundamental frequency is desired at bus 22,

the second alternative with only four branches of L-C is selected. This filter supplies 0.025 pu reactive power at bus 22. In practice, the second alternative may be preferable. It will be used hereafter for optimum filter realization.

In the case of unbalanced harmonic current sources, the network sequence components are used for representing the distribution feeder. Positive-sequence impedances are given in Appendix B. Negative-sequence impedances are assumed to be equal to positive-sequence impedances. Zero-sequence rectifier harmonic currents are assumed to be zero.

One case of unbalanced harmonic current source was simulated with one-phase (phase 'c') of the rectifier loads disconnected ($I_a = -I_b$, $I_c = 0$). The sequence components of current sources generated by such loads are $I_{a+} = (I_a/\sqrt{3})\angle -30°$, $I_{a-} = (I_a/\sqrt{3})\angle 30°$, and $I_{ao} = 0$ for positive-sequence harmonic currents (h = 7 and 13). For the 5-th and 11-th (negative-sequence) harmonic currents, I_{a+} and I_{a-} are interchanged. The results are exactly the same as the balanced harmonic source case, except the optimum filters here are only placed at phase a and b. As expected, a filter at phase 'c' is not necessary, since there is no zero-sequence harmonic sources and no distortion at phase c. The filters for phase a and b are shown in Table 4.2.

The *CTHD* with one optimum 3-phase filter at bus 22 is still above 1.0% for both balanced and unbalanced harmonic cases, and the highest *THD*s, particularly at buses on the upper feeder branch, are still above 2.5%. To reduce the *CTHD* to less than 1.0% on this two-branch feeder, it is required to place another filter on the upper feeder branch (one filter at each major feeder branch).

4.7.2 Two Filters

Table 4.3 shows the *CTHD* and the individual highest bus *THD* (averaged over the variable capacitor value range) for several possible placements of two filters. The result without any filter is the same as column 1 of Table 4.1. The second column of Table 4.3

shows the effect of tuned filters at two arbitrarily chosen buses, 8 and 25. The *CTHD* is reduced to 1.275%, but bus 20 still has 2.291% *THD*. This would represent a situation where two customers install filters tuned at or below harmonic frequencies without regard for other buses/customers. When tuned filters are moved to the capacitor banks near the feeder ends (buses 12 and 27, as suggested in [28,29]), harmonic distortion becomes even higher. The fourth column of the Table shows that *CTHD*, and *THD* at the most distorted bus, are reduced to less than 1.0%, when optimum filters found by minimizing eqn (4.6) and using the location search to find buses 3 and 27.

Table 4.3 Simulations with Two Filters for Balanced Harmonic Current Sources

	No Filter	Tuned Filters at Buses		Optimum Filters at Buses	
		8 and 25	12 and 27	3 and 27	3, 12 & 27
CTHD [%]	4.562	1.275	1.426	0.447	0.448
Most Distorted Bus	31	20	20	3	35
THD [%]	8.048	2.291	3.412	0.907	1.373

4.7.3 Sensitivity Analysis

For certain filter placement, the values of *CTHD* can be very sensitive to changes of component values (L or C) or changes of system frequency. In practice, capacitance changes more than inductance because of aging, changes of temperature and self heating, and may amount to several percent. To check sensitivity, the *CTHD* change corresponding to a 2% change of the filter capacitance or a 1% change of system frequency is calculated. If the value of *CTHD* increases to more than twice the minimum *CTHD*, the optimum filters and locations are indeed sensitive and other optimum filters and locations have to be found. However, the sensitivity problem can be avoided from the beginning of the location search by finding *CTHD* with a filter (shorted to ground) at each bus. Buses which, when

grounded, cause a substantial increase in *CTHD* are sensitive, and should be omitted from the search.

The *CTHD* in Table 4.3, with optimum filters placed at buses 3 and 27, is very sensitive to filter component values located at bus 3. If the 5-th harmonic filter is moved to bus 12, the *CTHD* is only slightly increased (to 0.448%, as shown in the last column of Table 4.3), but less sensitive to C or L. Therefore, buses 12 and 27 are selected for placing 5-th harmonic filter, and buses 3 and 27 for placing 7-th, 11-th and 13-th harmonic filters. Fig. 4.4 shows the plot of *THD* at each bus after placing these optimum filters versus

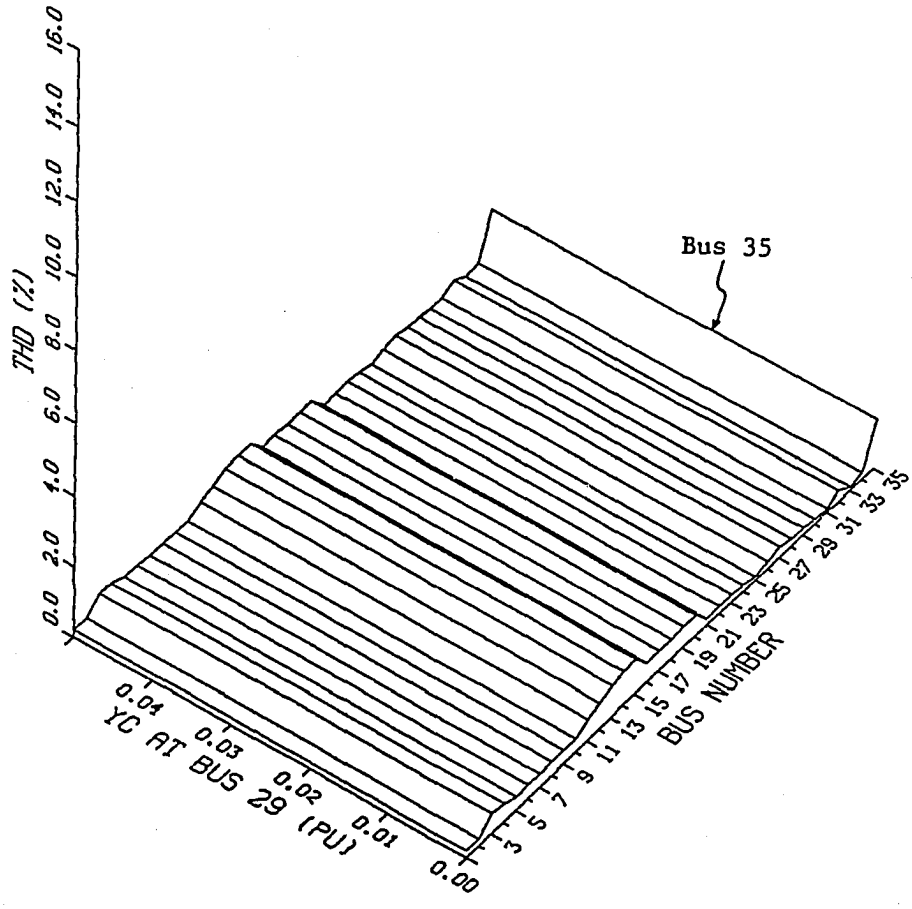

Fig. 4.4 3-D Plots of *THD*s versus Y_C at Bus 29 and Bus Number (After Placing Two Optimum Filters)

varying capacitive admittance at bus 29. From the figure, it can be seen that the highest *THD* (1.373%) now occurs at bus 35. With a 2% change of the filter capacitance or a 1% change of system frequency, the *CTHD* will only change to a maximum of 0.68%, with the highest *THD*, 1.6%, at bus 35. The optimum filter admittances and the realization of these filters are listed in Table 4.4. The total size of two 3-phase filters at buses 3, 12 and 27 as listed in Table 4.4 is 4,353.50 kVAR, which is comparable to the size of the single filter

Table 4.4 Optimum Filter Admittances and Realization at Buses 3, 12 and 27 (with One Variable Compensating Capacitor)

	Harmonic Order			
	5	7	11	13
Admittance [pu]				
at Bus 3	-------	3.083	4.177	3.776
at Bus 12	3.522	-------	-------	-------
at Bus 27	5.092	6.205	4.093	3.081
	Branch			
	L-C	L-C	L-C	L-C
At Bus 3 : Filter Rating = 969.50 kVAR (3-Phase)				
L [mH]		44.683	21.784	18.214
C [μF]		3.141	2.612	2.237
Pole Order		7.080	11.120	13.140
At Bus 12 : Filter Rating = 1,560.0 kVAR (3-Phase)				
L [mH]	16.324			
C [μF]	16.137			
Pole Order	5.168			
At Bus 27 : Filter Rating = 1,824.0 kVAR (3-Phase)				
L [mH]	40.011	21.880	20.410	19.399
C [μF]	6.887	6.424	2.789	2.101
Pole Order	5.053	7.075	11.118	13.140

optimization (4325.0 kVAR) from Table 4.2. With approximately same filter size (cost), the optimum two filter placement is preferable, because it reduces the harmonic distortion at every bus to about 1%.

The number of variable compensating capacitors may be increased to two, installed at buses 14 and 29, with both admittances varying from 0. to 0.05 pu (using 5 equal switching steps for each capacitor). The results are similar to Table 4.3. The *CTHD* before placing any filter is 5.053% and the highest *THD* (7.591%) occurs at bus 31. Using the location search algorithm, the optimum locations found including sensitivity checking are buses 12 and 27 for the 5-th and 7-th harmonic filter placements and buses 3 and 27 for the 11-th and 13-th harmonic filter placements. The *CTHD* found by minimizing eqn (4.6) is 0.491% with the highest *THD* of 1.407% at bus 35. With a 2% change of filter capacitance or a 1% change of system frequency, the *CTHD* increases to a maximum of 0.577% with the highest *THD*, 1.646%, at bus 35. The optimum filter admittances and the realization of these filters are listed in Table 4.5.

Table 4.5 Optimum Filter Admittances and Realization at Buses 3, 12 and 27
(with Two Variable Compensating Capacitors)

	Harmonic Order			
	5	7	11	13
Admittance [pu]				
at Bus 3	-------	-------	3.984	3.617
at Bus 12	3.604	1.952	-------	-------
at Bus 27	5.342	3.642	3.628	3.252
	Branch			
	L-C	L-C	L-C	L-C
At Bus 3 : Filter Rating = 433.79 kVAR (3-Phase)				
L [mH]			22.880	19.125
C [μF]			2.486	2.130
Pole Order			11.122	13.141
At Bus 12 : Filter Rating = 1,767.76 kVAR (3-Phase)				
L [mH]	23.963	28.132		
C [μF]	11.214	4.900		
Pole Order	5.117	7.144		
At Bus 27 : Filter Rating = 1,758.0 kVAR (3-Phase)				
L [mH]	36.184	34.056	22.786	18.871
C [μF]	7.610	4.122	2.497	2.159
Pole Order	5.055	7.080	11.120	13.140

CHAPTER 5

LC COMPENSATOR FOR VOLTAGE HARMONIC REDUCTION

From the energy user's point of view, the utility is an equivalent source that either supplies him with harmonics, or absorbs harmonics generated by him. In this study, both the equivalent source and load are considered to generate harmonics. It is assumed that the load harmonics are not sufficiently serious to suggest tuned filters, but when combined with source harmonics, the use of a pure capacitive compensator would degrade power factor and overload the equipment. The remedy explored here is insertion of a reactor in series with the local compensating capacitor. This will reduce the energy user's distortion, without regard for his neighbors. In such an arrangement, the *LC* compensator may actually have a lower voltampere rating (or cost) than that of a pure capacitive compensator.

In other attempts at optimizing the *LC* compensator [34,35], the main objective has been to maximize the load power factor. This may also reduce the total harmonic distortion of voltage and current, but it may not minimize them. In other words, the problem of minimizing voltage harmonic distortion is not solved by maximizing power factor.

In addition, it is necessary to consider randomly varying source harmonics and impedances. Fixed solutions for one harmonic source condition may not be optimal for another. Therefore, time variations of the harmonics and impedances must be considered in designing an optimum *C* [41,42] or *LC* compensator [35]. If the characteristics of these time-varying quantities are not known a priori, they can be either found by a microcomputer-based parameter estimator [43], or monitored by the method developed in Chapter 3.

In this chapter, a method is presented for minimizing the voltage total harmonic distortion (*THD*) at the load bus where it is desired to maintain a given displacement factor (fundamental power factor) with stochastic source harmonics and impedances [46]. An optimum fixed *LC* compensator will be selected that will minimize the expected value of

THD for a specified range of source harmonic and impedance values, while constraining the total size and cost of the compensation network.

The basic approach to harmonic reduction is first explained, and the cost function expression and analysis are discussed. Then, the optimization algorithm using the steepest descent method is presented. Finally, the simulation tests are performed, and the results, the expected values of *THD*s as function of compensator costs for different values of displacement factors, are compared with the performance and cost of pure capacitive compensation.

5.1 Basic Approach to Harmonic Reduction

Fig. 5.1(a) is a single-phase equivalent circuit of a bus with capacitive compensation, experiencing voltage harmonic distortion at harmonic order h because of a nonlinear voltage source, v_{sh}, and harmonic current sources within the load itself, i_{Lh}. Fig. 5.1(b) is the same bus, except that a series reactor, X_L, has been added to minimize voltage *THD* while X_C has been altered to maintain the displacement factor.

The Thevenin voltage source representing the utility supply and the harmonic current source representing the nonlinear load are

$$v_s(t) = \sum_h v_{sh}(t), \tag{5.1}$$

and

$$i_L(t) = \sum_{h>1} i_{Lh}(t), \tag{5.2}$$

where h is the order of harmonic present. The h-th harmonic Thevenin source and load impedances are

$$Z_{th} = R_{th} + j X_{th}, \tag{5.3}$$

and

$$Z_{lh} = R_{lh} + j X_{lh}. \tag{5.4}$$

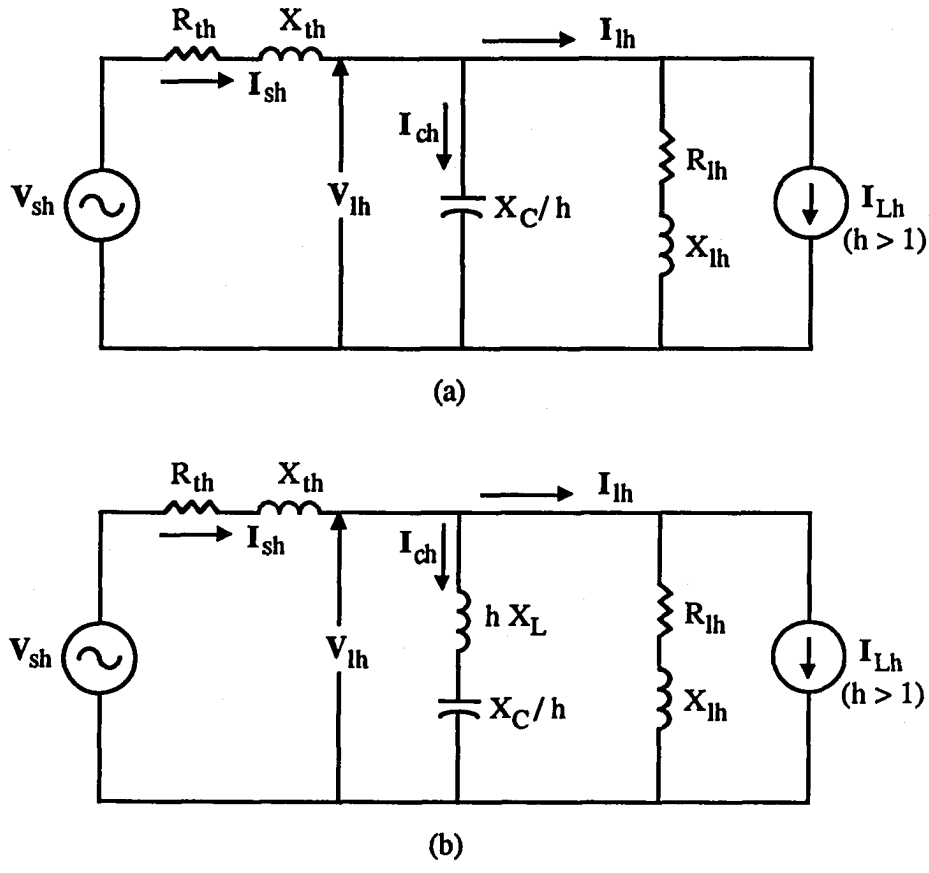

Fig. 5.1 Single-Phase Equivalent Circuit for h-th Harmonic
(a) With Capacitive Compensation, and
(b) With *LC* Compensation

The approach will be to minimize voltage harmonic distortion on the load by adjusting X_C and X_L while keeping the displacement factor constant and constraining the cost of the compensating circuit to a series of fixed values. This can be accomplished by minimizing a total cost function which represents a combination of *THD* and compensator cost:

$$K = c_f \ THD^2 + M \tag{5.5}$$

In this equation, M is the cost of X_C and X_L based on voltampere requirement, THD^2 is the voltage total harmonic distortion squared, and c_f is an arbitrary factor to

convert THD^2 to cost. c_f serves as a Lagrange multiplier in the optimization and need not be found explicitly. *THD* is squared to facilitate the minimization calculation. Although the total cost K generated by eqn (5.5) may have little meaning because of the difficulty in assigning a cost factor to *THD*, minimizing K for a range of c_f will provide a series of *THD*s, each with its corresponding minimum compensator cost. Minimum cost and *THD* can then be plotted with c_f as a parameter.

Since source harmonics and impedances are randomly time-varying quantities, eqn (5.5) has to be modified to accommodate a probabilistic cost and *THD*. K becomes $E(K)$, the expected value of cost, which is to be minimized. On the right-hand side of eqn (5.5), M must represent the most severe of the varying loadings to which X_C and X_L may be subjected, rather than the average. Thus, for the probabilistic case, eqn (5.5) becomes

$$E(K) = c_f \; E(THD^2) + M_{\max} \tag{5.6}$$

where $E(K)$ and $E(THD^2)$ are respectively the expected values of K and THD^2.

5.2 Cost Function Expression

With the *LC* compensator connected at the load terminals as shown in Fig. 5.1(b), the load voltage and compensator current for each harmonic frequency $h\,\omega_O$ are, respectively,

$$V_{lh} = \frac{V_{sh}(R_{clh} + j\,X_{clh}) - I_{Lh}[\,j\,(h\,X_L - X_C/h)\,(R_{tlh} + j\,X_{tlh})]}{A_{rh} + j\,A_{ih}}, \tag{5.7}$$

and

$$I_{ch} = \frac{V_{sh}(R_{lh} + j\,X_{lh}) - I_{Lh}(R_{tlh} + j\,X_{tlh})}{A_{rh} + j\,A_{ih}}, \tag{5.8}$$

where

$$X_L = \omega_o L,$$

$$X_C = \frac{1}{\omega_o C},$$

$$R_{tlh} = R_{th} R_{lh} - X_{th} X_{lh},$$

$$X_{tlh} = R_{th} X_{lh} + R_{lh} X_{th},$$

$$R_{clh} = - X_{lh} (h X_L - X_C / h),$$

$$X_{clh} = R_{lh} (h X_L - X_C / h),$$

$$A_{rh} = R_{tlh} - (X_{lh} + X_{th})(h X_L - X_C / h), \text{ and}$$

$$A_{ih} = X_{tlh} + (R_{lh} + R_{th})(h X_L - X_C / h). \qquad (5.9)$$

The voltage total harmonic distortion at the compensated load terminals is defined as in eqn (2.13),

$$THD = \frac{\left(\sum_{h>1} V_{lh}^2 \right)^{1/2}}{V_{l1}}. \qquad (5.10)$$

The compensator cost, M, in the second term of eqn (5.5) is defined as

$$M = U_L S_L + U_C S_C \qquad (5.11)$$

where U_L and U_C are, respectively, the cost of reactor and capacitor per kVAR, and considered to be constant parameters.

For reactors and capacitors, ratings are defined [47] as

$$S_L = \left(\sum_h I_{ch}^2 \right)^{1/2} \sum_h (I_{ch} h X_L) \quad kVAR \qquad (5.12)$$

and

$$S_C = \left(\sum_h I_{ch}^2 \right)^{1/2} \sum_h (I_{ch} X_C / h) \quad kVAR \qquad (5.13)$$

where I_{ch} is given in eqn (5.8). In eqns (5.12) and (5.13), the harmonic voltage magnitudes are added linearly to emphasize the effect of peak (as opposed to RMS) voltage on component rating or cost.

For randomly time-varying voltage source harmonics and source impedances, $E(THD^2)$ must be expressed as a function of X_C and X_L and of the statistics of random variables. Because distribution system harmonic generators are generally current sources, a positive correlation exists between source harmonic impedance X_{th} and R_{th}, and source harmonic voltage V_{sh}, which is a product of source impedances and Norton equivalent current sources. In the most extreme case, source voltage, source resistance and reactance are linearly correlated to each other at each harmonic order $h > 1$, that is, $V_{sh} = g_h X_{th}$ and $R_{th} = t_h X_{th}$, where g_h and t_h are constants for $h > 1$, and X_{th} is a random variable which varies linearly with frequency. Then, the expected value of V_{lh} (eqn (5.7)) squared can be written as

$$E(V_{lh}^2) = E\left(\frac{d_h X_{th}^2}{c_h X_{th}^2 + b_h X_{th} + a_h}\right) \tag{5.14}$$

where a_h, b_h, and c_h are functions of t_h, R_{lh}, X_{lh}, $h X_L$ and X_C/h; and d_h is a function of I_{Lh}, g_h, t_h, R_{lh}, X_{lh}, $h X_L$ and X_C/h. By definition,

$$E(V_{lh}^2) = \int_{-\infty}^{+\infty} f(X_{th})\, V_{lh}^2 \, dX_{th} \tag{5.15}$$

where $f(X_{th})$ is the probability density function of X_{th}. If the source reactance X_{th} is assumed to have a uniform distribution function with minimum value β_h and maximum value γ_h, eqn (5.15) becomes

$$E(V_{lh}^2) = \frac{d_h}{\gamma_h - \beta_h} \int_{\beta_h}^{\gamma_h} \frac{X_{th}^2}{c_h X_{th}^2 + b_h X_{th} + a_h} \, dX_{th} \tag{5.16}$$

By integration, $E(V_{lh}^2)$ for $h > 1$ can be calculated, and the expected value of THD^2 can be expressed as

$$E(THD^2) = \frac{\sum_{h>1} E(V_{lh}^2)}{V_{l1}^2} \tag{5.17}$$

M_{max} in eqn (5.6) is calculated in the same way as M in eqn (5.11), except that I_{ch} in eqns (5.12) and (5.13) assumes its maximum magnitude:

$$I_{ch} = V_{shmax}\left(\frac{R_{lh}^2 + X_{lh}^2}{A_{rh}^2 + A_{ih}^2}\right)_{max}^{1/2} + I_{Lh}\left(\frac{R_{tlh}^2 + X_{tlh}^2}{A_{rh}^2 + A_{ih}^2}\right)_{max}^{1/2} \tag{5.18}$$

where V_{shmax} is considered to be a priori known or found by measurement.

The expressions for $E(THD^2)$ and M_{max} are then substituted into eqn (5.6) which is minimized with respect to X_C and X_L for a range of c_f values.

5.3 Cost Function Analysis

To minimize $E(K)$ in eqn (5.6), it is necessary to find the optimum values, X_C^* and X_L^*, which cause the differential of $E(K)$ to vanish, i.e.,

$$dE(K) = \frac{\partial E(K)}{\partial X_C} dX_C + \frac{\partial E(K)}{\partial X_L} dX_L = 0. \tag{5.19}$$

However, X_C and X_L are related because the displacement factor of the load is to remain constant. To keep the fundamental frequency compensating current constant,

$$X_L - X_C = \text{constant}, \tag{5.20}$$

so that eqn (5.19) reduces to:

$$dE(K) = \frac{\partial E(K)}{\partial X_C} + \frac{\partial E(K)}{\partial X_L} = 0. \tag{5.21}$$

Since $E(K)$ is generally nonlinear and multimodal in the variables X_C and X_L, the condition in eqn (5.21) is not sufficient. Fig. 5.2 is a plot of $E(K)$ and $E(THD^2)$ versus X_L for the parameter values and load listed in Table 5.1, with a displacement factor of 0.78, $c_f = 5 \times 10^5$, and source harmonics and impedances varying with standard deviations σ = 30% and 10%, with uniform probability density functions. This figure shows a series of $E(K)$ minima separated by resonance peaks. These resonance peaks can be obtained by setting the imaginary part of the expected impedance seen from the Thevenin source to zero, resulting in a quadratic equation in X_C and X_L for any given harmonic order h,

$$A\left(hX_L - X_C/h\right)^2 + B\left(hX_L - X_C/h\right) + C = 0 \tag{5.22}$$

where

$$A = X_{th} + X_{lh},$$

$$B = R_{lh}^2 + X_{lh}^2 + 2X_{lh}X_{th},$$

$$C = X_{th}\left(R_{lh}^2 + X_{lh}^2\right), \tag{5.23}$$

and by taking the solution of quadratic equation (5.22) where the square root of the discriminant is positive. (The other solution corresponds to resonance between the load and the combination of source impedance and compensator). Note that for sufficiently large R_{lh} and/or X_{lh}, eqn (5.22) reduces to

$$hX_L - X_C/h + X_{th} = 0 \tag{5.24}$$

which then represents only the resonance condition between source impedance and compensator. Note that the resonance peaks broaden for increasing variance of X_l.

Immediately to the right of each $E(THD^2)$ peak are local minima where X_C and X_L act as a series filter, effectively grounding the corresponding harmonic. At these points, one harmonic voltage is eliminated at the bus, but large harmonic currents are attracted

down the distribution line through the compensator, so that the compensator cost (which subsumes a worst-case condition) is relatively high. An $E(K)$ minimum is found when X_L is such that compensator cost combined with THD, weighted by c_f, satisfies eqn (5.21).

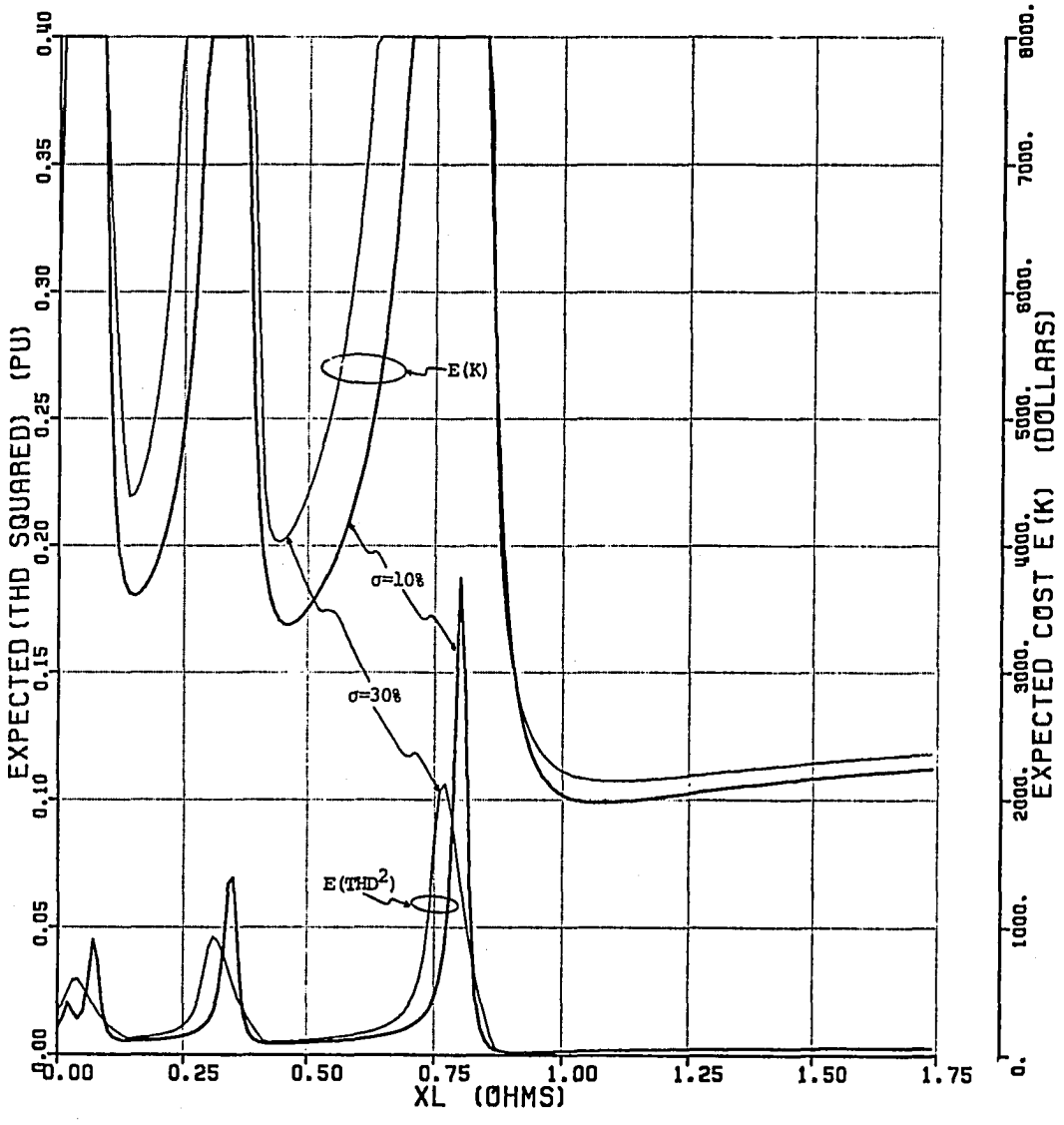

Fig. 5.2 Plot of $E(K)$ and $E(THD^2)$ versus X_L

—— $\sigma = 30\ \%$
—— $\sigma = 10\ \%$

Table 5.1 System Parameters and Source Harmonics

Parameters and Harmonics	Case 1	Case 2
R_{t1} [Ω]*	0.01154	0.01154
X_{t1} [Ω]	0.1154	0.1154
$E(X_{t5})$ [Ω]	0.557	0.557
$E(X_{t7})$ [Ω]	0.8078	0.8078
$E(X_{t11})$ [Ω]	1.2694	1.2694
$E(X_{t13})$ [Ω]	1.5002	1.5002
R_{l1} [Ω]**	1.7421	1.7421
X_{l1} [Ω]**	1.696	1.696
V_{s1} [V]	2400.	2400.
$E(V_{s5})$ [$\%V_{s1}$]	5.	1.
$E(V_{s7})$ [$\%V_{s1}$]	3.	7.
$E(V_{s11})$ [$\%V_{s1}$]	2.	2.
$E(V_{s13})$ [$\%V_{s1}$]	1.	1.
I_{L5} [$\% I_{s1}$]	5.	5.
I_{L7} [$\% I_{s1}$]	3.	3.
I_{L11} [$\% I_{s1}$]	2.	2.
I_{L13} [$\% I_{s1}$]	1.	1.
U_L [$/kVAR]	2.	2.
U_C [$/kVAR]	2.	2.

* $R_{th} = t_h X_{th}$, where $t_h = 0.1$ for $h > 1$.

** R_{lh} is frequency independent and $X_{lh} = h X_{l1}$, where h is the order of the harmonic.

To find the global minimum of $E(K)$, it is necessary to find the local minimum between each pair of potential resonance points. Then, by comparing the local minima, a global minimum can be found. The method used to find the minimum between each pair of resonance points is the steepest descent method, which has the advantage of relatively fast convergence. It should be noted that the $E(K)$ global minimum does not necessarily occur in the range of X_L enclosed by the lowest order resonance peaks. A different content in the voltage or load harmonic sources may result in a global minimum that occurs between higher order resonance peaks.

5.4 Optimization Algorithm

Since the cost function $E(K)$ is constrained by a constant displacement factor, that is, $X_L - X_C$ = constant, optimization of $E(K)$ reduces to minimization of eqn (5.6) with respect to one of the variables (X_C or X_L). X_L is used as the variable and X_C is replaced by (X_L - constant).

Following the steepest descent algorithm given in Appendix A, the algorithm used in this study can be summarized as follows:

1. Select a value for the displacement factor.
2. Select a starting value for c_f.
3. Start at an initial point $X_L^{(0)}$ in the range of values enclosed by the lowest order resonance peaks which will not create a resonance condition as stated in eqn (5.24).
4. Calculate the gradient vector at $X_L^{(i)}$:

$$N(X_L^{(i)}) = \frac{dE(K)}{dX_L}(X_L^{(i)}). \tag{5.25}$$

5. If $$\left\| N(X_L^{(i)}) \right\| < \varepsilon \tag{5.26}$$

where ε is a preselected small positive number (ε << 1), then terminate the iterative procedure, output the optimum value X_L^* and go to step 6. If the stopping criterion

(5.26) is not satisfied, then generate a new point given by

$$X_L^{(i+1)} = X_L^{(i)} - \tau\, N(X_L^{(i)}) \tag{5.27}$$

where τ (> 0) is the step size which has to be judiciously selected. Then, replace $X_L^{(i)}$ by $X_L^{(i+1)}$ and return to step 4.

6. If the range of X_L values is not the last one, go to the next range and return to step 3. If the range of X_L is the last one, compare all the local minima and find the global minimum cost.

Repeat the above process for a given range of c_f values and plot the expected *THD* versus the minimum compensator cost with c_f as parameter. Finally, repeat the whole process for different values of the displacement factors.

5.5 Simulation Tests

Two cases of an industrial plant were simulated using the optimization method. The numerical data in case 1 were primarily taken from an example in Ref. [32]. The load consists of an inductive three-phase load which is 5100 kW with a displacement factor of 0.717 and harmonic current sources as listed in Table 5.1. The 60 cycle supply bus voltage and Thevenin impedance are 4.16 kV line to line and (0.01154 + j 0.1154) Ω, respectively. Fundamental parameters and load harmonics were assumed to be time-invariant quantities. The voltage source harmonics and Thevenin impedances for h > 1 were assumed to be randomly time-varying quantities with their expected values as listed in Table 5.1 and their standard deviations σ equal to 30%. The source and load in case 1 were arbitrarily chosen to have the same harmonic content as suggested in Ref. [32]. These harmonic magnitudes are generally independent. In case 2, the fifth harmonic voltage source was decreased to 1% and the seventh harmonic voltage source was increased to 7% of V_{s1}. In both cases, the range of c_f values is 0.0 - 10^6.

The parameter values of case 1 were then applied to the optimization algorithm with U_C and U_L taken equal to 2 \$/kVAR. This generated several plots of minimum expected *THD* versus compensator cost for a range of c_f values with different displacement factors (varying from 0.75 to 1.0) as displayed in Fig. 5.3. Note that for each displacement factor, the expected *THD* decreases with increased compensator cost until saturation occurs, at which point a cost increment results in a much smaller decrease in *THD*.

The circles indicate the minimum expected *THD*s that can be achieved by pure capacitive compensation with the corresponding displacement factors. For higher displacement factors than those shown, the expected *THD*s and the corresponding compensator costs are much higher, and some of them are off the figure's scale. It is observed that the *LC* compensator achieves a much lower expected *THD* than a capacitor alone at the same displacement factor, and an *LC* compensator may cost less than a capacitor.

Another simulation with different voltage source harmonic contents (Table 5.1) was performed (case 2). The optimization result is shown in Fig. 5.4. The expected *THD*s are higher than those in Fig. 5.3 with the same compensator cost. This is to be expected because the voltage source harmonic contents in case 2 are higher than in case 1. Although the prescribed values of the X_L in case 1 were below the 5-th harmonic, for case 2, the optimal values of X_L fell between the 5-th and 7-th harmonic. The expected *THD*s achieved by using a pure capacitive compensator (marked by the circles) are much higher than with the *LC* compensator at the same displacement factor.

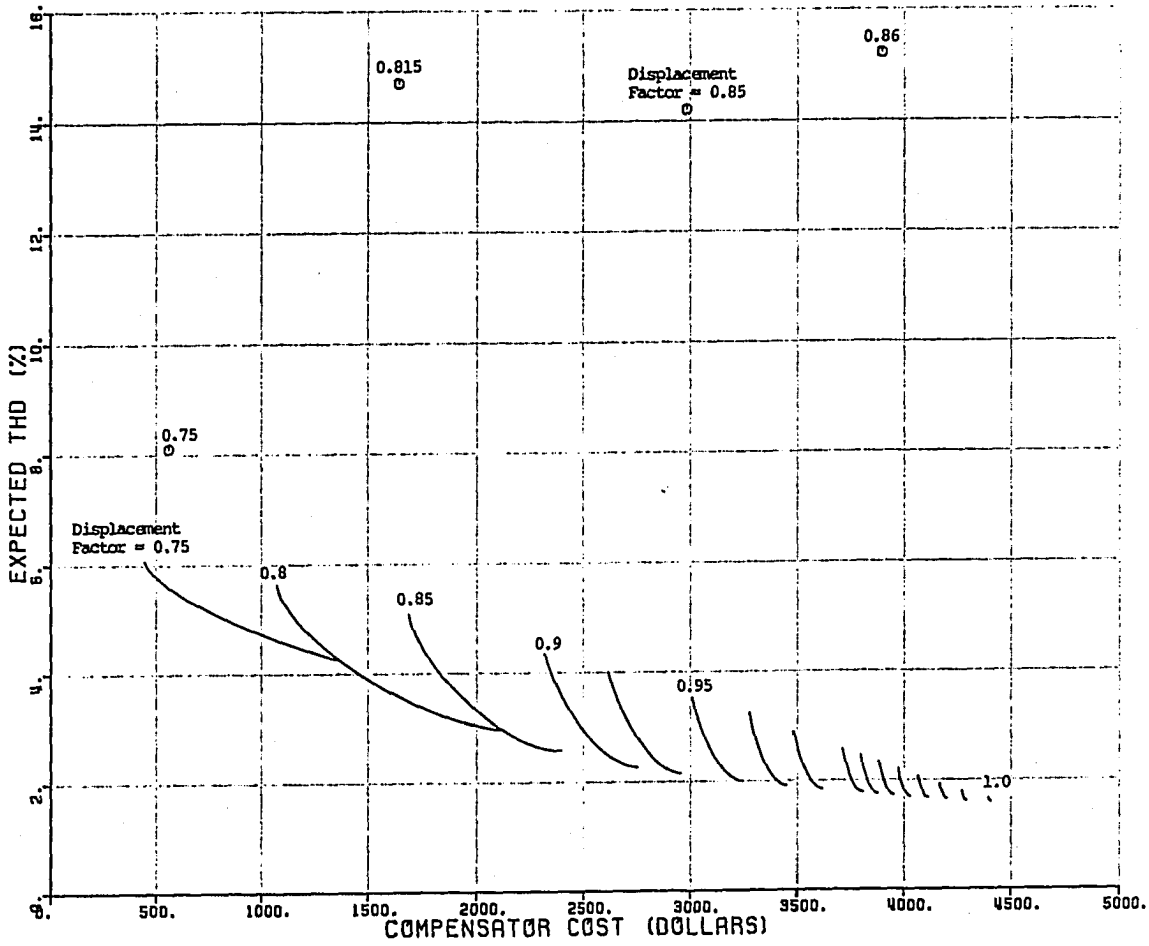

Fig. 5.3 Expected *THD* versus Compensator Cost for Case 1
o o o Expected *THD* by Capacitor Only

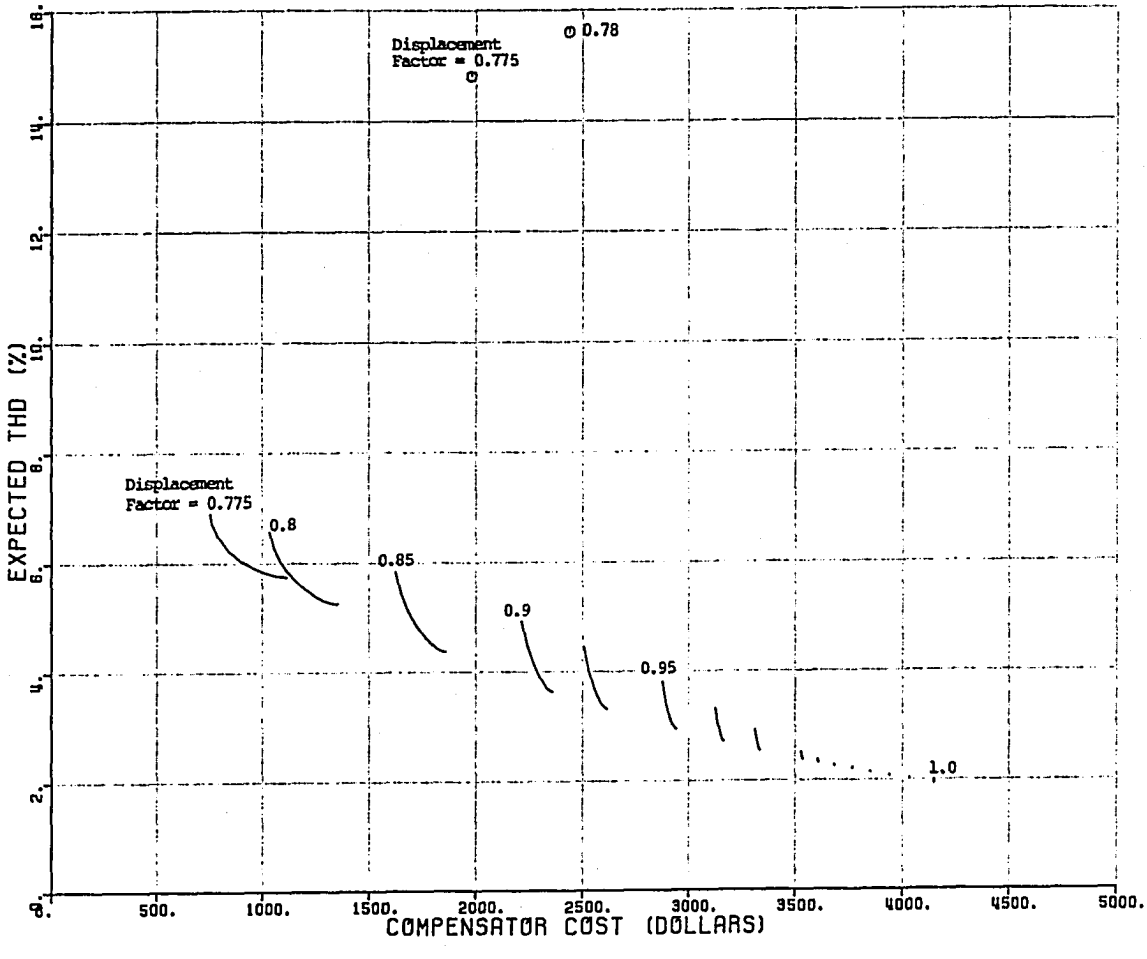

Fig. 5.4 Expected *THD* versus Compensator Cost for Case 2
o o o Expected *THD* by Capacitor Only

CHAPTER 6
CONCLUSIONS

In this dissertation, a method for monitoring and identifying harmonic sources using relatively few harmonic measurements has been presented. Two techniques for reducing voltage harmonic distortion, one from the energy supplier's point of view and the other from the user's point of view, have also been discussed. The conclusions of the work presented in those studies are:

1. In cases where harmonic measuring instruments are only installed at few buses, neural networks in conjunction with state estimation can be used to monitor harmonic sources and also to identify an additional unknown harmonic source. A structured neural network with multiple parallel two-layer feedforward nets can be applied to make initial estimates of harmonic sources. The neural network estimates can then be used as pseudomeasurements for harmonic state estimation. The results of simulations from an IEEE 14-bus example system showed that the state estimator pulled the pseudomeasurements closer to the correct values at known harmonic generation buses and successfully identified and monitored a "suspected" harmonic source which had not previously been measured.
2. From an energy supplier's point of view, a feeder filtering technique for selecting and placing optimum filters on distribution feeders with variable compensating capacitors can be used to reduce distortion of all buses. The case of distributed, balanced or unbalanced harmonic sources was also considered. A sample procedure on a 35-bus distribution feeder showed that optimum filters chosen and placed in the prescribed manner reduced voltage harmonic distortion at every bus to a lower value than that achieved by a filter designed to reduce distortion at only a single bus. The optimum filters are also more effective than the conventional resonant shunts (tuned filters) placed to minimize total feeder distortion.

Best results are obtained when optimum filters are placed at selected buses with one filter at each major feeder branch. The results showed that the filter components at each feeder branch for different harmonic frequencies need not be at the same bus. The optimum locations are not always at the capacitor banks farthest from the substation. The optimum filters are tuned slightly above harmonic frequency, as opposed to the usual practice of tuning them slightly below harmonic frequency.

3. From an energy user's point of view, a displacement factor can be maintained while reducing voltage harmonic distortion at his own bus, if a reactor is inserted in series with the local compensating capacitor to form an *LC* compensator. The optimal reactance value can be found by minimizing a cost function including total harmonic distortion and total compensator cost. For time-varying cases, the cost function is derived from a probabilistic model of the Thevenin source harmonic voltages and impedances. Plots of simulation tests showed that a series reactor may provide a more cost effective remedy for voltage harmonics than merely detuning the original pure capacitive compensation. Compared with pure capacitive compensation, *LC* compensation may provide a higher displacement factor, or a lower total harmonic distortion, for the same cost. In any case, voltage harmonic distortion levels are reduced below those found with capacitance alone.

Recommendations for future research efforts include:

- Study of time variations and unbalances of harmonic sources and system parameters in designing optimum filters on a distribution system.
- Development of faster methods of finding optimum filter admittances and locations.
- Real-time on-line closed loop control of a harmonic reduction strategy on a distribution system with varying harmonics and system parameters.
- Improved methods of applying expert systems in harmonic identification for use with on-line harmonic control.

REFERENCES

[1] IEEE Working Group on Power System Harmonics, "Power System Harmonics: An Overview", *IEEE Transactions on Power Apparatus and Systems*, Vol. PAS-102, No. 8, August 1983, pp. 2455-2460.

[2] R. P. Stratford, "Harmonic Pollution on Power Systems - A change in philosophy", *IEEE Transactions on Industry Applications*, Vol. IA-16, No.5, September/October 1980, pp.617-623.

[3] R. E. Owen, M. F. McGranaghan, J. M. King, J. R. Vivirito and W. R. Vincent, *Study of Distribution System Surge and Harmonic Characteristics*, EPRI EL-1627, Project 1024-1, Electric Power Research Institute, Palo Alto, CA, November 1980.

[4] J. Arrillaga, D. A. Bradley and P.S.Bodger, *Power System Harmonics*, John Willey & Sons, Inc., New York, 1985.

[5] T. J. E. Miller, *Reactive Power Control in Electric Systems*, John Willey & Sons, Inc., New York, 1982.

[6] E. W. Kimbark, *Direct Current Transmission*, John Willey & Sons, Inc., New York, 1971.

[7] A. A. Mahmoud (Ed.), *Power System Harmonics*, IEEE Tutorial Course, No. 84 EH0221-2-PWR, 1984.

[8] G. Lemieux, "Power System Harmonic Resonance - A Documented Case", *Proceedings of Third International Conference on Harmonics in Power Systems*, Nashville, Indiana, September 28 - October 1, 1988, pp. 61-65.

[9] T. H. Ortmeyer, K. R. Chakravarthi and A. A. Mahmoud, "The Effects of Power System Harmonics on Power System Equipment and Loads", *IEEE Transactions on Power Apparatus and Systems*, Vol. PAS-104, No. 9, September 1985, pp. 2555-2563.

[10] Y. Baghzouz and Owen T. Tan, "Harmonic Analysis of Induction Watthour Meter Performance", *IEEE Transactions on Power Apparatus and Systems*, Vol. PAS-104, No. 2, February 1985, pp. 399-406.

[11] W . F. Horton and S. Goldberg, "The Effect of Harmonics on the Operating Points of Electromechanical Relays", *IEEE Transactions on Power Apparatus and Systems*, Vol. PAS-104, No. 5, May 1985, pp.1178-1188.

[12] A. M. Sharaf, "Harmonic Interference from Distribution Systems", *IEEE Transactions on Power Apparatus and Systems*, Vol. PAS-101, No. 8, August 1982, pp. 2975-2981.

[13] IEEE Working Group on Power System Harmonics, "Power Line Harmonic Effects on Communication Line Interference", *IEEE Transactions on Power Apparatus and Systems*, Vol. PAS-104, No. 9, September 1985, pp. 2578-2587.

[14] D. Xia and G. T. Heydt, "Harmonic Power Flow Studies, Part I: Formulation and Solution, and Part II: Implementation and Practical Application", *IEEE Transactions on Power Apparatus and Systems*, Vol. PAS-101, No. 6, June 1982, pp.1257-1270.

[15] G. T. Heydt, W. M. Grady and D. Xia, *Harmonic Power Flow Studies, Vol. 1: Theoretical Basis*, EPRI EL-3300, Project 1764-7, Electric Power Research Institute, Palo Alto, CA, November 1983.

[16] G. T. Heydt, W. M. Grady and D. Xia, *Harmonic Power Flow Studies, Vol. 2: Users' Guide*, EPRI EL-3300-CCM, Project 1764-7, Electric Power Research Institute, Palo Alto, CA, November 1983.

[17] D. J. Pileggi, N. H. Chandra and A. E. Emanuel, "Prediction of Harmonic Voltages in Distribution Systems", *IEEE Transactions on Power Apparatus and Systems*,, Vol. PAS-100, No. 3, March 1981, pp. 1307-1315.

[18] M. F. McGranaghan, R. C. Dugan and W. L. Sponsler, "Digital Simulation of Distribution System Frequency Response Characteristics", *IEEE Transactions on Power Apparatus and Systems*, Vol. PAS-100, No. 3, March 1981, pp. 1362-1389.

[19] A. A. Mahmoud and R. D. Shultz, "A Method for Analyzing Harmonic Distribution in AC Power Systems", *IEEE Transactions on Power Apparatus and Systems*, Vol. PAS-101, No. 6, June 1982, pp. 1815-1824.

[20] McGraw Edison Power Systems Co., " V-HARM (TM) - The Harmonics Verdict - Power System Harmonics Simulation and Analysis Program", Cannonsburg, PA, May 1988.

[21] J. P. Tamby, V. I. John, "Q'HARM - A Harmonic Powerflow Program for small Power Systems", *IEEE Transactions on Power Systems*, Vol. 3, No. 3, August 1988, pp. 949-955.

[22] M. F. McGranaghan, J. H. Shaw and R. E. Owen, "Measuring Voltage and Current Harmonics on Distribution Systems", *IEEE Transactions on Power Apparatus and Systems*, Vol. PAS-100, No.7, July 1981, pp. 3599-3608.

[23] M. F. McGranaghan, "Instrumentation and Methodology for Power System Harmonic Measurements", *International Conference on Harmonics in Power Systems*, Worcester Polytechnic Institute, Worcester, Massachusetts, Oct 22-23, 1984, pp. 213-219.

[24] D. M. Luke, A. M. Sharaf and M. Bin Awan, "A Microprocessor Based Power System Harmonic Analyzer with Application to Harmonic Model Identification", *International Conference on Harmonics in Power Systems*, Worcester Polytechnic Institute, Worcester, Massachusetts, Oct 22-23, 1984, pp. 199-202.

[25] G. E. Littler, "A Digital Harmonic Analyzer for Electrical Power Systems", *Proceedings of Third International Conference on Harmonics in Power Systems*, Nashville, Indiana, September 28 - October 1, 1988, pp. 122-126.

[26] G. T. Heydt, "Identification of Harmonic Sources By a State Estimation Technique", *IEEE Transactions on Power Delivery*, Vol. 4, No. 1, January 1989, pp. 569-576.

[27] D. A. Gonzales and J. C. McCall, "Design of Filters to Reduce Harmonic Distortion in Industrial Power Systems", *Conference Proceedings of IAS Annual Meeting*, October 6-11, 1985, pp.361-370.

[28] R. C. Dugan and C. D. Ko, "Analyzing and Controlling Harmonic Distortion on Distribution Feeders", *International Conference on Harmonics in Power Systems*, Worcester Polytechnic Institute, Worcester, Massachusetts, Oct 22-23, 1984, pp. 38-44.

[29] R. C. Dugan and D. T. Rizy, *Harmonic Considerations for Electrical Distribution Feeders*, Report No. ORNL/Sub/81-95011/4, Oak Ridge National Laboratory, Oak Ridge, TN, March 1988.

[30] M. F. McGranaghan, R. C. Dugan, J. A. King and W. T. Jewell, "Distribution Feeder Harmonic Study Methodology", *IEEE Transactions on Power Apparatus and Systems*, Vol. PAS-103, No. 12, December 1984, pp. 3663-3671.

[31] T. Hiyama, M. S. A. A. Hamman and T. H. Ortmeyer, "Distribution System Modeling with Distributed Harmonic Sources", *IEEE Transactions on Power Delivery*, Vol. 4, No.2, April 1989, pp. 1297-1304.

[32] R. F. Chu and R. H. Avendano, "A Direct Method for Identifying the Optimal Power Factor Correction in Nonsinusoidal Systems", *IEEE Transactions on Power Apparatus and Systems*, Vol. PAS-104, No. 4, April 1985, pp. 959-964.

[33] G. G. Richards, O. T. Tan and L. S. Czarnecki, "Comments on 'Considerations on the Reactive Power in Nonsinusoidal Situations", *IEEE Transactions on Instrumentation and Measurement*, Vol IM-35, No.3, September 1986, pp. 365-366.

[34] G. G. Richards, O. T. Tan, P. Klinkhachorn and N. I. Santoso, "Cost Constrained Power Factor Optimization with Source Harmonics Using LC Compensators", *IEEE Transactions on Industrial Electronics*, Vol. IE-34, No. 2, May 1987, pp. 266-270.

[35] G. G. Richards, P. Klinkhachorn, O. T. Tan and R. K. Hartana, "Optimal LC Compensators for Nonlinear Loads with Uncertain Nonsinusoidal Source and Load Characteristics", *IEEE Transactions on Power Systems*, Vol. 4, No. 1, February 1989, pp. 30-36.

[36] L. S. Czarnecki, "Minimisation of Distorted Power of Nonsinusoidal Sources Applied to Linear Loads", *Proc. IEE*, Part C, Vol. 128, No. 4, July 1981, pp. 208-210.

[37] L. S. Czarnecki, "Considerations on the Reactive Power in Nonsinusoidal Situations", *IEEE Transactions on Instrumentation and Measurement*, Vol IM-34, No.3, September 1985, pp. 399-404.

[38] L. S. Czarnecki, "Minimisation of Reactive Power Under Nonsinusoidal Conditions", *IEEE Transactions on Instrumentation and Measurement*, Vol IM-36, No. 1, March 1987, pp. 18-22.

[39] N. Taylor, "Harmonic Standards and Recommendations", *International Conference on Harmonics in Power Systems*, University of Manchester, Institute of Science and Technology, September 1981, pp. 118-131.

[40] Z. S. Mouneimne and L. R. Denning, "Converter Harmonics in DC Transportation Power Supplies", *International Conference on Harmonics in Power Systems*, Worcester Polytechnic Institute, Worcester, Massachusetts, Oct 22-23, 1984, pp. 132-136.

[41] R. T. Saleh and A. E. Emanuel, "Optimum Shunt Capacitor for Power Factor Correction at Busses with Lightly Distorted Voltage", *IEEE Transactions on Power Delivery*, Vol. PWRD-2, No. 1, January 1987, pp. 165-173.

[42] D. Raonic, D. Cyganski and A. E. Emanuel, "Power Factor Compensation at Buses with Slightly Distorted Voltage Due to Random Harmonics", *IEEE Transactions on Power Delivery*, Vol. 4, No. 1, January 1989, pp. 502-507.

[43] P. Klinkhachorn, R. K. Hartana and B. Huner, "Microcomputer Based Estimator for Power System Parameters in the Presence of Harmonics", *Proceeding IEEE Southeastcon 1988*, Knoxville, Tennessee, April 10-13, 1988, pp. 529-532.

[44] R. K. Hartana and G. G. Richards, "Harmonic Source Monitoring and Identification Using Neural Networks", accepted for presentation at *IEEE PES Winter Meeting*, Feb 4-9, 1990, Atlanta, Georgia.

[45] R. K. Hartana and G. G. Richards, "Optimum Filter Design for Distribution Feeders with Multiple Harmonic Sources", submitted to *International Conference on Harmonics in Power Systems*, Budapest Technical University, Budapest, Hungary, October 4-6, 1990. (Also considered for publication in *IEEE Transactions on Power Systems*).

[46] R. K. Hartana and G. G. Richards, "Comparing Capacitive and LC Compensators for Power Factor Correction and Voltage Harmonic Reduction", *Electric Power Systems Research*, Vol. 17, No. 1, 1989, pp. 57-64.

[47] IEEE Std. 519-1981, *IEEE Guide for Harmonic Control and Reactive Compensation of Static Power Converters*, IEEE Publication, 1981.

[48] A. D. Graham and E. T. Schonholzer, "Line Harmonics of Converters with DC-Motor Loads", *IEEE Transactions on Industry Applications*, Vol. IA-19, No. 1, January/February 1983, pp. 84-93.

[49] R. L. Smith Jr. and R. P. Stratford, "Power System Harmonics Effects from Adjustable-Speed Drives", *IEEE Transactions on Industry Applications*, Vol. IA-20, No. 4, July/August 1984, pp. 973-977.

[50] R. De Vre, "Harmonic Distortion Produced in Supply Networks by Television Receivers and Light Dimmers", *IEE Conference Publications*, No. 210, 1981, pp. 121-128.

[51] J. A. Orr, A. E. Emanuel and D. J. Pileggi, "Current Harmonics, Voltage Distortion and Powers Associated with Battery Chargers, Part I: Comparisons Among Different Types of Chargers", *IEEE Transactions on Power Apparatus and Systems*, Vol. PAS-101, No. 8, August 1982, pp. 2703-2710.

[52] A. K. Wallace, E. S. Ward and A. Wright, "Sources of Harmonic Currents in Slip-Ring Induction Motors", *Proc. IEE*, Vol. 121, No. 12, December 1974, pp. 1495-1500.

[53] P. M. Anderson, *Analysis of Faulted Power Systems*, The Iowa State University Press, Ames, Iowa, 1976.

[54] Owen T. Tan and P. Hillers, *Power System Harmonic Analysis*, Technical Report, prepared for Louisiana Power and Light Co., Louisiana State University, Baton Rouge, Louisiana, September 1981.

[55] G. T. Heydt, *Computer Analysis Methods for Power Systems*, Macmillan Publishing Co., New York, 1986.

[56] H. Sasaki and T. Machida, "A New Method to Eliminate AC Harmonic Currents by Magnetic Flux Compensation", *IEEE Transactions on Power Apparatus and Systems*, Vol. PAS-90, No. 5, September/October 1971, pp. 2009-2019.

[57] A. Mirbod, G. G. Richards, O. T. Tan and R. K. Hartana, *Harmonic Flux Compensation in Distribution Systems*, Technical Report, prepared for LSU - Utilities Power Research Consortium, Louisiana State University, Baton Rouge, Louisiana, October 1984.

[58] B. M. Bird, J. F. Marsh and P. R. McLellan, "Harmonic Reduction in Multiplex Convertors by Triple-Frequency Current Injection", *Proc. IEE*, Vol. 116, No. 10, October 1969, pp. 1730-1734.

[59] A. Ametani, "Generalised Method of Harmonic Reduction on AC/DC Convertors by Harmonic Current Injection", *Proc. IEE*, Vol. 119, No. 7, July 1972, pp. 857-864.

[60] J. F. Baird and J. Arrillaga, "Harmonic Reduction in DC Ripple Reinjection", *Proc. IEE*, Vol. 127, Part C, No. 5, 1980, pp. 294-303.

[61] H. S. Patel and R. G. Hoft, "Generalized Techniques of Harmonic Elimination and Voltage Control in Thyristor Inverters: Part I - Harmonic Elimination", *IEEE Transactions on Industry Applications*, Vol. IA-9, No. 3, May/June 1973, pp. 310-317.

[62] R. E. Larson, W. F. Tinney and J. Peschon, "State Estimation in Power Systems, Part I: Theory and Feasibility", *IEEE Transactions on Power Apparatus and Systems*, Vol. PAS-89, March 1970, pp. 345-352.

[63] F. C. Schweppe and E. J. Handschin, "Static State Estimation in Electric Power Systems", *Proc. of IEEE*, Vol. 62, No. 7, July 1974, pp. 972-982.

[64] D. J. Sobajic and Yoh-Han Pao, "Artificial Neural-Net Based Dynamic Security Assessment for Electric Power Systems", *IEEE Transactions on Power Systems*, Vol. 4, No. 1, February 1989, pp. 220-228.

[65] S. Ebron, D. L. Lubkeman and M. White, "A Neural Network Approach to the Detection of Incipient Faults on Power Distribution Feeders", *IEEE PES Transmission and Distribution Conference*, April 2-7, 1989, New Orleans, Louisiana, paper No. 89 TD 377-3 PWRD.

[66] N. I. Santoso and O. T. Tan, "Neural-Net Based Real-Time Control of Capacitors Installed on Distribution Systems", *IEEE PES Summer Meeting*, July 9-14, 1989, Long Beach, California, Paper No. 89 SM 768-3 PWRD.

[67] R. Rosenblatt, *Principles of Neurodynamics: Perceptrons and the Theory of Brain Mechanisms*, Spartan Books, Washington, D.C., 1961.

[68] R. P. Lippmann, "An Introduction to Computing with Neural Nets", *IEEE Acoustics Speech and Signal Processing Magazine*, April 1987, pp. 4-22.

[69] D. E. Rumelhart, G. E. Hinton and R. J. Williams, "Learning Internal Representations by Error Propagation", in *Parallel Distributed Processing: Explorations in the Microstructure of Cognition* (eds. Rumelhart and McClelland), Vol. I, MIT Press, 1986, pp. 318-362.

APPENDIX A

STEEPEST DESCENT ALGORITHM

The Steepest Descent algorithm for an objective function with six variables, $CTHD(Y_{p\varphi}, Y_{q\varphi})$, $\varphi = a, b, c$, can be summarized as follows:

1. Select an initial point $(Y_{p\varphi}^{(0)}, Y_{q\varphi}^{(0)}), \varphi = a, b, c.$

2. Calculate the unit gradient vectors at $(Y_{p\varphi}^{(i)}, Y_{q\varphi}^{(i)})$:

$$G_{p\varphi}(Y_{p\varphi}^{(i)}, Y_{q\varphi}^{(i)}) = \frac{\frac{\partial CTHD}{\partial Y_{p\varphi}}(Y_{p\varphi}^{(i)}, Y_{q\varphi}^{(i)})}{\|G\|},$$

$$G_{q\varphi}(Y_{p\varphi}^{(i)}, Y_{q\varphi}^{(i)}) = \frac{\frac{\partial CTHD}{\partial Y_{q\varphi}}(Y_{p\varphi}^{(i)}, Y_{q\varphi}^{(i)})}{\|G\|}, \quad \varphi = a, b, c, \tag{A.1}$$

where $\|G\| = \sqrt{\sum_{\varphi=a,b,c} \left\{ \left(\frac{\partial CTHD}{\partial Y_{p\varphi}} \right)^2 + \left(\frac{\partial CTHD}{\partial Y_{q\varphi}} \right)^2 \right\}}$

is the total gradient vector.

3. If $\left\| G_{p\varphi}(Y_{p\varphi}^{(i)}, Y_{q\varphi}^{(i)}) \right\| < \varepsilon$ and $\left\| G_{q\varphi}(Y_{p\varphi}^{(i)}, Y_{q\varphi}^{(i)}) \right\| < \varepsilon$ (A.2)

where ε is a preselected small positive number (ε <<< 1), then terminate the iterative procedure, output the optimum value $(Y_{p\varphi}^{*}, Y_{q\varphi}^{*})$, $\varphi = a, b, c$, and stop. If the stopping criterion (A.2) is not satisfied, then generate a new point given by

$$Y_{p\varphi}^{(i+1)} = Y_{p\varphi}^{(i)} - \delta\, G_{p\varphi}(Y_{p\varphi}^{(i)}, Y_{q\varphi}^{(i)}),$$

$$Y_{q\varphi}^{(i+1)} = Y_{q\varphi}^{(i)} - \delta\, G_{q\varphi}(Y_{p\varphi}^{(i)}, Y_{q\varphi}^{(i)}), \quad \varphi = a, b, c, \tag{A.3}$$

where δ (>0) is the step size which has to be judiciously selected. Then, replace $(Y_{p\varphi}^{(i)}, Y_{q\varphi}^{(i)})$ by $(Y_{p\varphi}^{(i+1)}, Y_{q\varphi}^{(i+1)})$ and return to step 2.

APPENDIX B

NETWORK IMPEDANCES FOR A DISTRIBUTION SYSTEM

Source impedance: $Z_S = (0.126 + j\ 1.3863) \times 10^{-3}$ pu

Transformer impedance: $Z_{tr} = (8.9477 + j\ 134.72) \times 10^{-3}$ pu

Line impedances [pu]:

From	To	R_l ($\times 10^{-3}$)	X_l ($\times 10^{-3}$)	X_C($\times 10^{3}$)
1	2	1.764	2.647	5.573
2	3	44.739	79.647	12.519
3	4	5.671	10.082	98.903
4	5	16.383	29.238	34.104
5	6	2.521	3.907	3.715
5	7	32.262	57.467	17.351
7	8	2.773	5.041	197.807
8	9	3.151	4.915	2.972
8	10	8.444	24.197	65.940
8	11	11.342	32.262	49.451
11	12	9.578	17.139	58.178
12	13	22.684	40.328	24.726
13	14	10.208	18.147	54.946
14	15	9.074	16.131	61.815
4	16	13.611	24.197	41.210
16	17	9.578	17.139	58.178
17	18	2.647	4.033	3.570
17	19	24.323	43.352	23.000
19	20	5.711	10.082	98.900
1	21	1.008	1.638	8.920
21	22	36.169	64.146	15.950
22	23	16.383	29.238	34.100
23	24	33.396	59.483	16.763
24	25	19.786	47.637	28.300
25	26	32.892	78.891	17.100
26	27	7.940	19.030	70.650
27	28	11.342	27.220	49.451
28	29	3.403	8.192	164.840
29	30	22.054	53.056	25.400
30	31	20.920	50.410	26.730
23	32	39.067	93.888	14.330
25	33	7.940	19.030	70.645
26	34	9.578	23.188	58.200
1	35	20.794	445.872	5.740

Load Impedances [pu]:

From	To	R_L	X_L
2	0	1920.00	57.59
3	0	155.69	4.68
4	0	117.56	3.53
5	0	59.99	1.80
6	0	164.56	4.94
7	0	457.14	13.71
8	0	234.15	7.02
9	0	101.05	3.04
10	0	107.88	3.24
11	0	167.41	5.03
13	0	218.17	6.54
14	0	120.00	3.60
15	0	37.12	1.11
16	0	118.03	3.54
17	0	70.42	2.12
18	0	87.28	2.62
19	0	296.84	8.91
20	0	96.01	2.89
22	0	1797.76	53.98
23	0	423.64	12.70
24	0	149.99	4.50
25	0	121.51	3.64
26	0	124.13	3.73
28	0	116.60	3.50
29	0	488.29	14.64
30	0	91.42	2.75
31	0	285.22	8.56
32	0	164.56	4.94
33	0	51.90	1.56
34	0	89.73	2.70

Capacitor reactances [pu]:

From	To	X_C
12	0	20.00
13	0	20.00
14	0	20.00
15	0	20.00
17	0	40.00
19	0	40.00
27	0	40.00
29	0	20.00
35	0	8.57

Note:

V_{base} = 13.8 kV and VA_{base} = 24 MVA.

VITA

Rutisurhata K. Hartana was born on February 17, 1958, in Jakarta, Indonesia. He attended elementary and secondary schools in Jakarta, Indonesia, graduating from Canisius high school with honors in December 1975. In January of 1976, he entered Trisakti University in Jakarta, Indonesia, and received his Engineer Degree in Electrical Engineering in June 1982. He was a part time instructor for Laboratories at Trisakti University. In August of 1982, he entered Louisiana State University in Baton Rouge, Louisiana, USA, and received his Master of Science degree in Electrical Engineering in December 1983. He has held a research assistantship from January 1984 to the present, and a teaching assistantship from January 1985 to the present in the Electrical and Computer Engineering Department. He is a student member of the Institute of Electrical and Electronics Engineers. Presently, he is a candidate for the degree of Doctor of Philosophy in Electrical Engineering.

DOCTORAL EXAMINATION AND DISSERTATION REPORT

Candidate: Rutisurhata K. Hartana

Major Field: Electrical Engineering

Title of Dissertation: Harmonic Measurement and Reduction in Power Systems

Approved:

Major Professor and Chairman

Dean of the Graduate School

EXAMINING COMMITTEE:

Date of Examination:

10/2/89